Vagus nerve stimulation accelerates motor learning through cholinergic modulation.

Jordan Hickman*[1], Spencer Bowles*[1,2], Xiaoyu Peng*[1,2], W. Ryan Williamson[3], Rongchen Huang[1,2], Kayden Washington[1], Dane Donegan[1,2], Cristin G Welle[1,2,4]

[1]Department of Physiology and Biophysics, [2]Department of Neurosurgery, [3]IDEA Core, University of Colorado School of Medicine. * These authors contributed equally to this work. [4]Corresponding author. Email: cristin.welle@cuanschutz.edu.

Abstract

Vagus nerve stimulation (VNS) is a novel therapeutic option to treat a broad and rapidly expanding set of neurologic conditions. While classically used to treat epilepsy and depression, more recently VNS has received FDA approval as a therapeutic option for stroke rehabilitation and is under preclinical and clinical investigation for other disorders. Despite benefits across a diverse range of neurological disorders, the mechanism for how VNS influences central nervous system circuitry is not well described. A deeper understanding of the influence of VNS on neural circuits and activity is needed to optimize the use of VNS therapy.

To define the complex dynamics between VNS, neuronal activity, plasticity and behavior, we performed chronic VNS in mice during the learning of a dexterous motor task, and leveraged genetic tools to perform optogenetic circuit dissection and longitudinal *in vivo* imaging calcium activity in cortical neurons. We find VNS has the most robust effect on motor learning when paired with successful movement outcome, while randomized stimulation impairs learning, consistent with VNS serving as a reinforcement cue. In motor cortex, VNS paired with movement outcome selectively modulates neurons that are representing outcome, but not other movement-related neurons. Finally, cholinergic signaling from basal forebrain is required both for VNS-driven improvements in motor learning and the effects on neural activity in M1. This suggests that the effect of VNS on motor learning is mediated by cholinergic signaling, and also presents a novel role for cholinergic signaling in endogenous motor learning. These data imply that VNS therapy may be mediated by augmenting reinforcement cues with precisely-timed cholinergic neuronal activity, presenting strategies for optimizing the use of VNS to treat neurologic conditions.

Introduction

Vagus Nerve Stimulation (VNS) is currently used in clinical care to treat epilepsy[1,2] and depression[3], but novel responsive stimulation paradigms are being explored to treat a broad and growing range of neurologic injuries [4–6]. Recently, VNS paired with motor rehabilitation was approved by the FDA for the treatment of motor deficits associated with stroke [6]. Preclinical and early clinical studies suggest that paired VNS speed functional recovery from other neurologic conditions, including spinal cord injury, peripheral nerve injury and traumatic brain injury [7–9]. Despite the wide-ranging etiology of these conditions, the therapeutic model is similar: VNS is paired with a relevant rehabilitation protocol. It is hypothesized that this precise timing of stimulation drives targeted circuit plasticity for recovery from injury[5,10]. Yet, the lack of a clear circuit mechanism limits optimization of VNS therapy to treat neurologic injury.

The circuitry that mediates VNS effects on central nervous system plasticity remains poorly understood. Vagus nerve afferents terminate in the brainstem nucleus tractus solitarius (NTS) [11], which in turn activates many subcortical and cortical brain regions, including major subcortical neuromodulatory nuclei [12–14]. Lesions of major neuromodulatory centers, including the cholinergic basal forebrain (BF), limit VNS-driven cortical map plasticity [15,16] and functional rehabilitation after nerve damage [9]. In addition, the cholinergic basal forebrain has been indicated as necessary for motor learning[17], and phasic cholinergic signals are thought to play critical roles in reinforcement learning and outcome representation [18,19]. Together, these suggest a possible role for phasic cholinergic signaling in mediating the effects on VNS-driven learning, although this remains to be substantiated. In addition to activation of neuromodulatory nuclei, VNS has a well-document effect of decorrelating neural activity in cortex and across other brain areas[20–22]. Recent in vivo imaging studies have confirmed a broad, excitatory effect of VNS across multiple cortical regions[14]. Yet, the effects of VNS are specific to a paired sensory or motor stimuli, suggesting VNS may confer more specific modulation of key neural circuits.

To understand the mechanisms by which VNS can modulate neural circuits to optimally enhance motor behavior, we compared the effect VNS timing on skilled reach learning and then used optogenetic cholinergic circuit manipulation, kinematic analysis, and *in vivo* calcium imaging in the motor cortex of freely behaving animals to dissect the circuit that underlies VNS action. Paired-VNS accelerated the learning of a dexterous reach task, but only when applied as a reinforcement signal for a successful reach (Success VNS). Cholinergic neural activity in BF was required for the effects of VNS on motor learning. Improved reach performance by Success VNS was achieved by increased reach consolidation over learning, which also depended on cholinergic signaling. Finally, VNS altered specific neural populations relevant to reach representation in primary motor cortex, and the effects of VNS in M1 were mitigated by cholinergic antagonists. Our results reveal that VNS serves as a reinforcement signal during early learning and acts

through cholinergic signaling to modulate the activity of behaviorally-relevant neural populations in motor cortex, resulting in increased reach consolidation and improved motor learning.

Results

VNS enhances motor skill learning when paired with successful task outcome

To induce motor rehabilitation and cortical plasticity, VNS must be paired with motor output[23,24] at a relatively short latency[8], yet a single optimal pairing protocol has not been identified. To explore the optimal timing of VNS during skilled motor learning, we applied multiple VNS pairing protocols as freely moving mice learned a dexterous forelimb reaching task. Using a newly developed chronic VNS approach for mice [25], we implanted a microfabricated stimulation cuff on the left cervical vagus nerve (**Fig. 1a**) connected to a skull-mounted headcap. Mice were trained daily for 14 days (**Fig. 1b**,**c**,).

To identify an optimal VNS pairing strategy for enhancing dexterous motor learning, we explored four pairing protocols (**Fig. 1b**). First, to test if VNS drives plasticity by increasing widespread cortical excitation and inducing general arousal during a session [14], VNS was applied at pseudo-random intervals (Random VNS) during the 20-minute training session. Alternatively, VNS may modulate short-term attention, or influence spike timing dependent plasticity [26]. To test this, VNS was applied at the initiation of a subset of reach movements (Reach VNS). A third option is that VNS may augment reward or reinforcement pathways, and is better paired with movement outcome [27,28]. To explore this option, a third cohort received VNS after successful reach completion (Success VNS). The surgical control cohort was implanted with stimulation cuffs and connected to a stimulation isolation unit that was turned 'off' (Sham VNS). Current amplitude was the same across groups and the number of stimulation trains delivered during training sessions did not correlate with reach success (**Supplementary Fig.1a-c**).

Animals in all cohorts (Sham VNS, Random VNS, Reach VNS, and Success VNS) learned the dexterous reach task (Sham VNS: $p=0.0001$, Random VNS $p=0.0001$, Reach VNS $p=0.0002$, Success VNS $p=0.001$; Supplementary **Fig. 2b-e**). Neither Random nor Reach VNS altered the success rate of the animals relative to Sham VNS (Random, 47.4% ± 3.9%; Reach 53.6% ± 3.5%; Sham, 46.3% ± 3.2%; **Fig. 1g**). However, Success VNS improved the success rate over Sham VNS (59.2% ± 3.1% vs 46.3% ± 3.2% **Fig. 1g**), demonstrating for the first time, that paired VNS can accelerate motor learning in healthy animals.

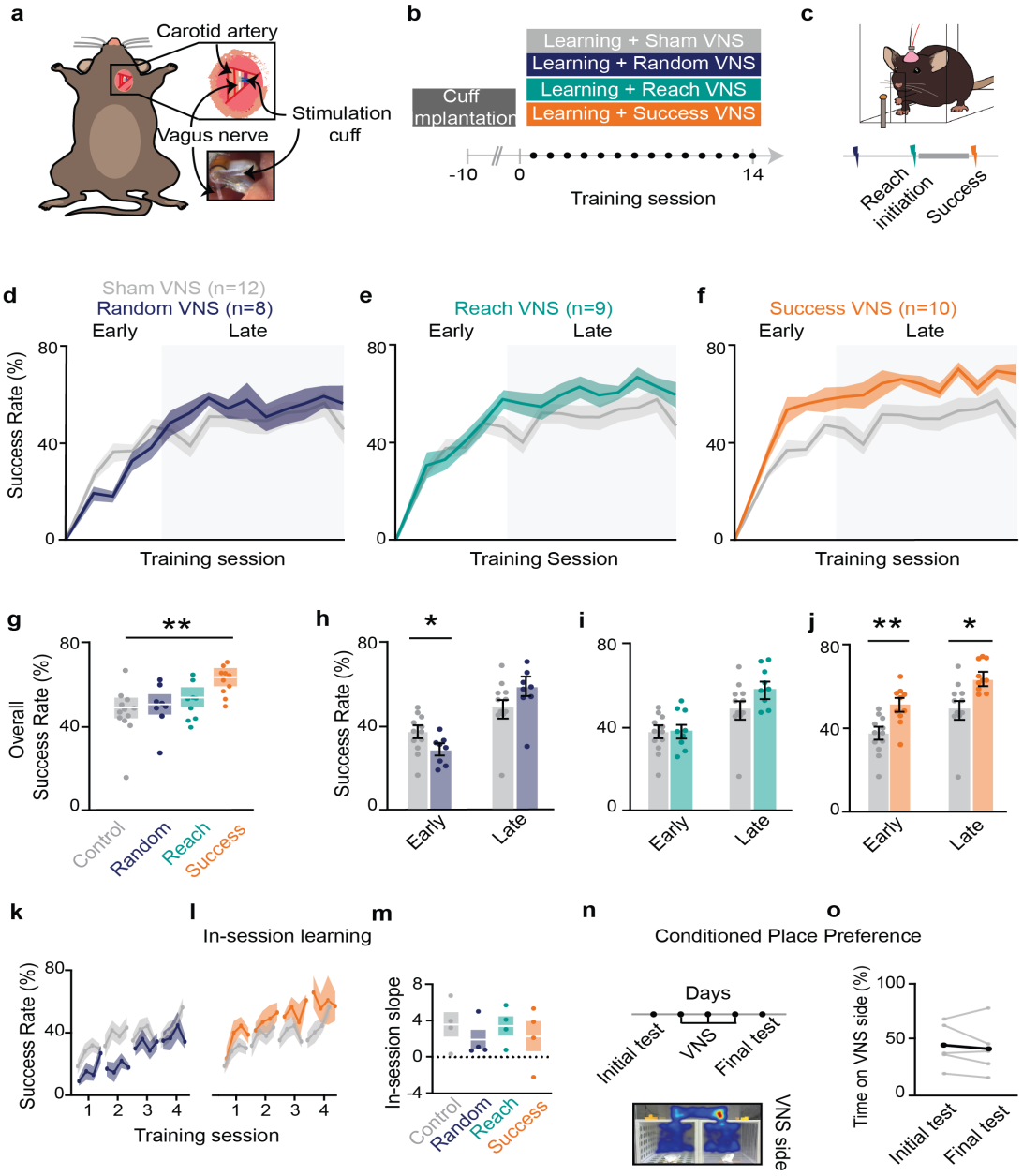

Figure 1 | VNS modulates forelimb reach learning and requires temporally specific stimulation. a-c, Illustration of VNS surgery, behavior timeline, and stimulation protocol. **d-f,** Random VNS, Reach VNS, and Success VNS success rate across 14 sessions of training. **g,** Comparison of mean performance across all days between control and stimulated groups (Success VNS: p=0.0065, f=9.24, Random VNS: p>0.05, Reach VNS: p>0.05, Student T test). **h,** Comparison of mean success rate for control and Random VNS mice during early (p=0.028, f=7.07, Student T test) and late learning (p>0.05). **i,** Comparison of mean success rate for control and Reach VNS mice during early and late learning (p>0.05). **j,** Comparison of mean success rate for control and Success VNS mice during early (p=0.0031) and late learning (p=0.0126). **k,l,** in-session learning trajectories for each group. **m,** Comparison of within session learning between all groups across 4 days of learning. **n, o,** VNS mice performed a conditioned place preference test after 3 days being stimulated in one of two distinct rooms. *p < 0.05, **p < 0.01, ***p< 0.001 bars and error bars represent the mean ± s.e.m.

In addition, these results indicate the importance of pairing VNS as a reinforcement cue during skilled motor learning.

VNS serves as a reinforcement cue during early learning but is not inherently rewarding.

Prior work on learning of a dexterous reach has suggested a multiphasic approach to learning, with distinct early and late learning phases [29,30], yet the time of early to late transition has not been empirically demonstrated. Using a Weibull growth curve nonlinear model (55.49% ± 6.81) we identified early learning as days 1-4 and late learning as days 5-14 (**Supplementary Fig. 2a)**. We next examined if VNS exerted distinct effects during different learning stages. Interestingly, despite having no effect on the 14-day average results, Random VNS impaired early learning (27.3% ± 7.3% versus 37.4% ± 8.9%), but performance recovered during late learning (**Fig. 1h)**. Reach VNS had no influence on success rates at any phase of learning (**Fig. 1i)**. Success VNS increased success rates during the early phase and late phase (early: 50.6% ± 9.4% versus 37.4% ± 8.9%; late: 63.6% ± 6.9 versus 49.6% ± 13.2% **Fig. 1j)**. These data suggest that VNS paired with a successful outcome accelerates learning and increases the final proficiency of a forelimb task, while random application of stimulation temporarily impairs learning during early learning.

To determine if VNS alters within-session learning or between-session learning [31], training session data was grouped into 4 blocks of 5 trials each (**Fig. 1k,l)**, and then the within-session learning slope was quantified over the first 4 days (**Fig.1m**). Within-session learning slope was not significantly different between conditions, suggesting that Success VNS likely operates by promoting between-session learning. One means by which Success VNS might confer learning benefit is through activation of a classical reward system [32]. To determine if VNS serves as a rewarding or aversive stimulus, we used a well-documented behavioral assessment of reward, the conditioned place preference test (CPP) (**Fig. 1n)**. Implanted mice were introduced to two rooms with distinct visual and olfactory cues, with VNS applied in one room. On the final day probe session, mice spent equal time in the conditioned (stimulated) room on the initial and final test days (44.8% ±2.0% and 41.4% ± 2.3%, **Fig.1o**), indicating that VNS is not inherently rewarding or aversive.

VNS confers both short-term performance benefits during the execution of known tasks.

Despite a lack of evidence for within-session learning, we wanted to confirm the behavioral results were due to learning, and not short-term modulation of attention. Since Success VNS is applied after reach outcome, the success rate of trials that immediately follow a stimulation (post-success) were compared to

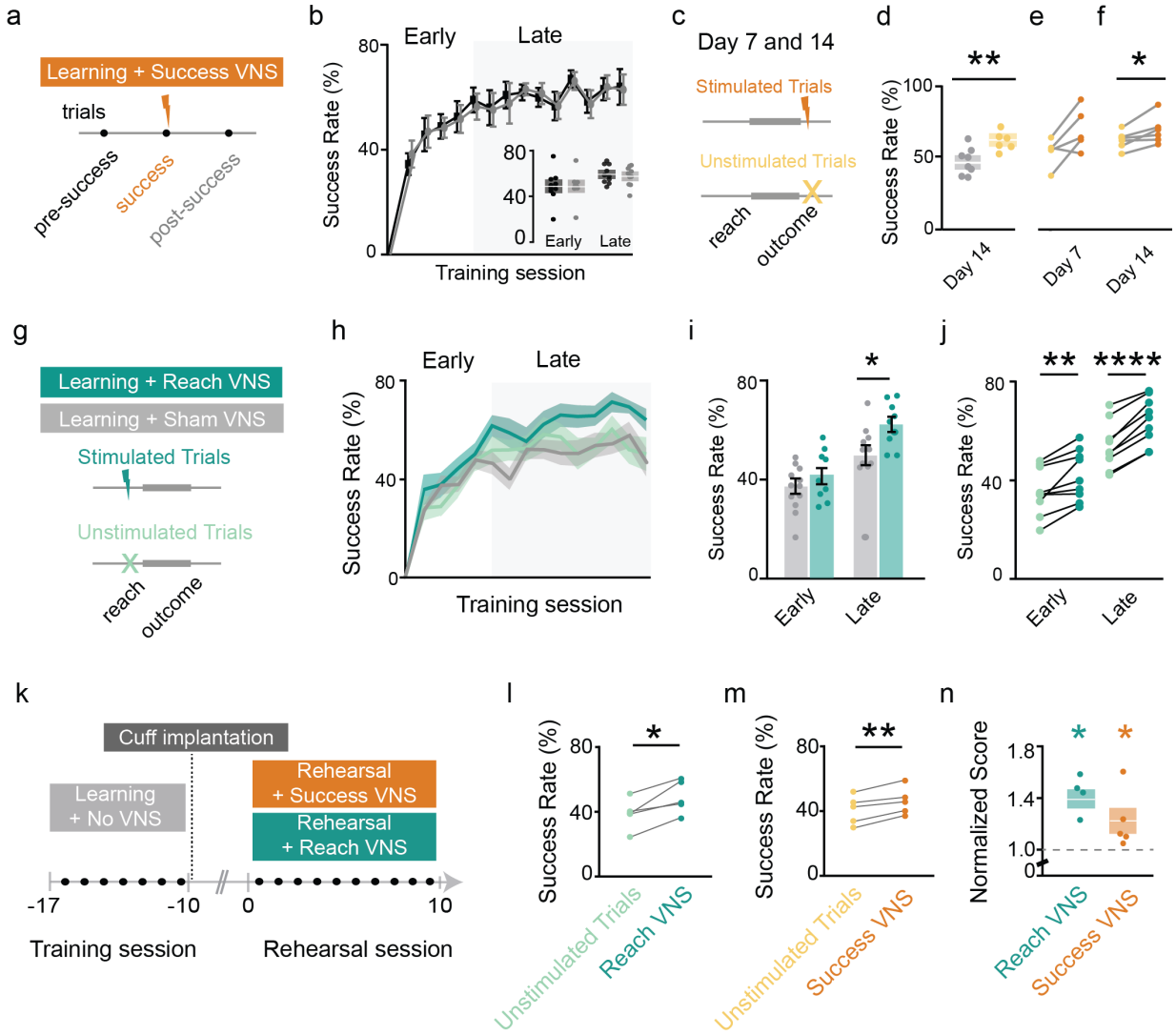

Figure 2 | VNS improves success rate within sessions and in learned mouse during rehearsal of forelimb reach task. a, trials before and after a stimulated success are investigated in success VNS **b,** Comparison of success rate for reaches preceding or following stimulated reach. **c,** For Success VNS, day 7 and 14 trials are divided into equal blocks of unstimulated and stimulated trials. **d,** Comparison of unstimulated (light orange) and sham (grey) trials on day 14 (p=0.0059, t=3.34, Student's T test). **e&f,** Comparison of stimulated (dark orange) and unstimulated (light orange) trials on days 7 & 14 (Day 7: p>0.05; Day 14: p=0.0499, t=2.57, Ratio paired t test). **g,** Reach VNS schematic **h,** Success rates across learning training sessions for Sham (grey), Stimulated Reach VNS (dark green), and Unstimulated Reach VNS (light green). **i,** Comparison of stimulated Reach VNS and Sham VNS trials in early (p>0,05) and late learning (p=0.024, t=2.47, Student's T test). **j,** Comparison between stimulated Reach VNS and unstimulated Reach VNS trails in early (p=0.004, t=3.98, paired t test) and late learning (p<0.0001, t=10.08, paired t test). **k,** Success VNS and Reach VNS applied during rehearsal of reach task in naively trained mice. **l,** Stimulated Reach VNS trials improve success rate during rehearsal (p=0.015, t=4.058, paired t test). **m,** Stimulated Success VNS trials improve success rate during rehearsal (p=0.005, t=5.62, paired t test). **n,** Normalized improvement of stimulated Reach VNS (p=0.047, t=3.56) and stimulated Success VNS trials (p=0.028, t=4.16) compared to unstimulated trials (Sidak's multiple comparison's test in RM one-way ANOVA). *p < 0.05, **p < 0.01, ***p < 0.001; bars and error bars represent the mean ± s.e.m.

those immediately prior (pre-success), and there was no trial-level difference (**Fig. 2a,b**). We next compared the response to Success VNS to an unstimulated probe trial block included on days 7 and 14(**Fig. 2c**). The success rate for unstimulated trials on Day 14 was greater than Sham VNS (61.9% ± 6.3% versus

46.6% ± 9.2% **Fig. 2d)**, suggesting that Success VNS led to stimulation-independent, lasting learning. Yet also, performance during stimulated blocks was greater than unstimulated blocks on day 14 (69.7% ± 10.2% and 61.9% ± 6.3; **Fig. 2f**), but not day 7 (**Fig. 2e)**, implying a short-term performance benefit in mice that have learned the task, in addition to the improved learning.

To further explore potential short-term benefits of VNS, we took advantage of the Reach VNS trial design, which allowed subgroup analysis of only stimulated or unstimulated reaches (**Fig. 1g**). The success rate of only stimulated trials is greater than sham during late learning (64.0% ± 9.4% versus 50.8% ± 13.7) (**Fig. 2i),** while unstimulated trials are not different from sham. Paired analysis for individual animals shows a higher success rate for stimulated trials compared to unstimulated trials in both the early and late phase (early: 41.9% ± 10.2% vs 35.3% ± 9.7; late: 64.0% ± 9.4% vs 53.7% ± 9.5%) (**Fig. 2j).** Taken together, Reach VNS provides a short-term performance boost for stimulated over unstimulated trials throughout learning. Yet, like Success VNS, Reach VNS most effectively modulates short-term performance for motor skills that are already learned.

Finally, to confirm that VNS augments the performance of a known task, paired VNS was applied to animals already proficient in the skilled reaching task (**Fig. 2k)**. Both Success VNS (**Fig. 2m**) and Reach VNS (**Fig. 2l**), delivered on alternate days for 10 days, improved performance over trial blocks without VNS (Success VNS 46.0% ± 8.5% vs 40.8% ± 8.9%; Reach VNS 49.0% ± 10.2% versus 38.8% ± 9.5%), confirming that either pairing protocol is sufficient to modulate the short-term performance of a known task.

VNS drives neural activity in the basal forebrain (BF)

Cholinergic neuromodulation is associated with reinforcement-driven plasticity[18,33] and is required for motor learning[34–36]. The basal forebrain (BF) is the source of cortically-projecting cholinergic neurons[37], however the response of BF neurons to VNS *in vivo* remains unknown. To address this question, tetrodes were implanted into the BF of mice with VNS cuffs (**Fig. 3a**). Extracellular activity was recorded during VNS in awake animals. (30 Hz, 0.6 mA, 100us pulse, 500ms train). Neurons in the BF displayed an altered firing rate following VNS onset, as compared to baseline (**Fig. 3b,c**). VNS elicited activation or suppression in 43% of recorded units, with 61% of activated units showing increased activity (**Fig. 3d**) which began during the stimulation train and persisted after stimulation ended (**Fig. 3e**).

The BF contains multiple neuronal cell types [38], so opto-tagging was used to identify cholinergic BF neurons[39] and interrogate their VNS response. Acute recordings were performed in anesthetized ChAT-ChR2 transgenic mice (B6.Cg-Tg(Chat-COP4*H134R/EYFP,Slc18a3)6Gfng/J) (**Fig. 3f**). Optrodes were

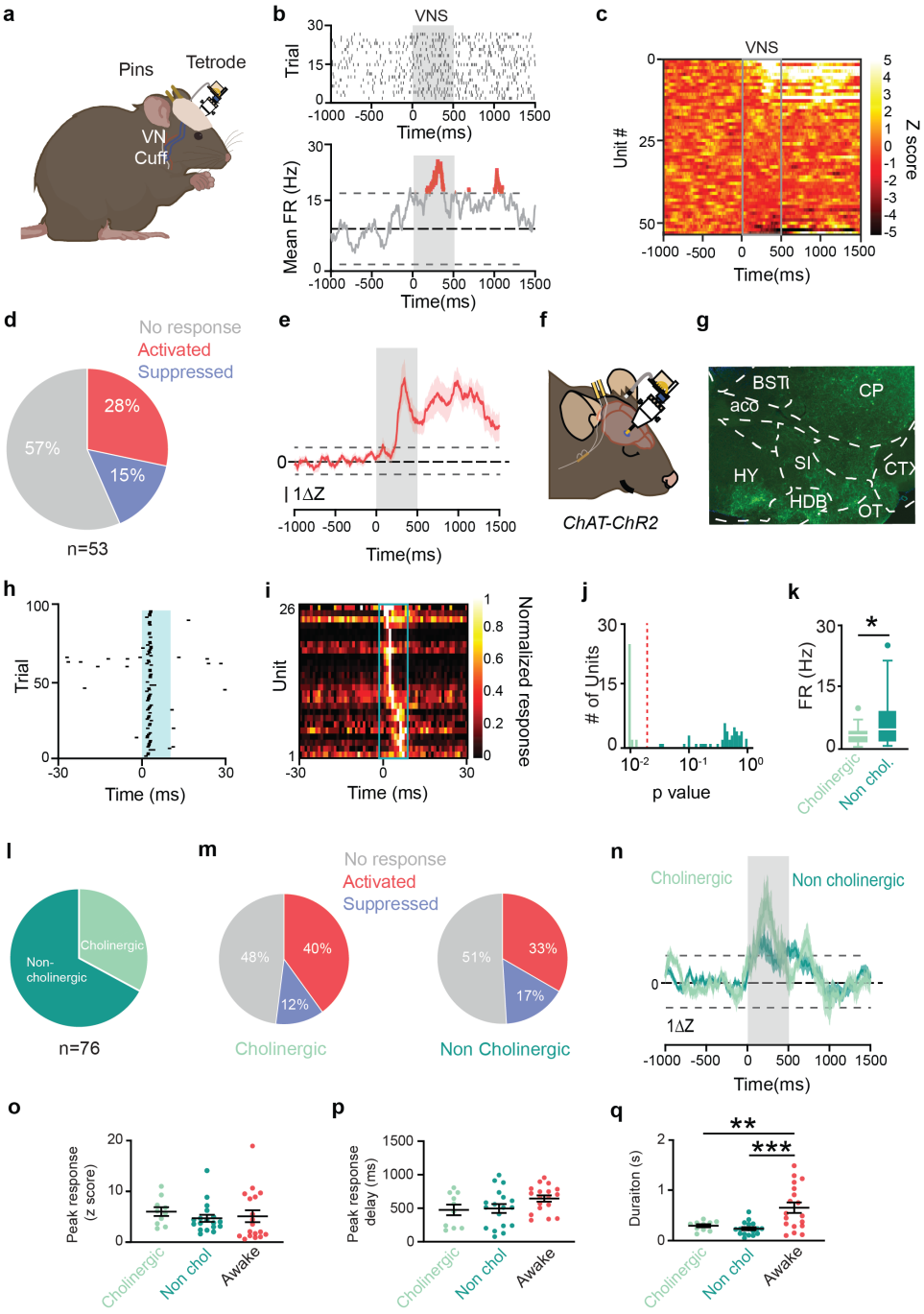

Figure 3 | VNS drives BF neural activity in anesthetized and awake mice.
a, Tetrodes were implanted in the left BF of mice and recordings were obtained during awake behavior. **b,** Example raster (top) and average firing rate from a response to VNS. Grey box denotes stimulus delivery. **c,** Average responses of all recorded neurons to VNS (grey box). **d,** Percent of neurons that respond to VNS (N = 5 mice, 53 neurons). **e,** Average activity of all 'activated' neurons in response to VNS. Dashed lines mark significance, shading represents SE. **f,** Extracellular recordings were obtained using optrodes while under light anesthesia. **g,** Optrodes were targeted at the HDB in *ChAT-ChR2* transgenic mice. Green fluorescence denotes the presence of ChR2. **h,** Example cholinergic neuron responding consistently to pulses of 488 nm light. **i,** Average activity of all cholinergic neurons during opto-tagging. Each row represents a neuron. **j,** Stimulus-associated latency tests (SALT) separate light responsive neurons from non-light responsive neurons. **k,** Mean baseline FR of cholinergic and non-cholinergic neurons (p=0.013, N = 5 mice, 53 neurons). **l,** Percent of neurons categorized as cholinergic (light green) and non-cholinergic (dark green) (N = 6 mice, 76 neurons). **m,** Percent of units that are VNS-responsive in cholinergic (left) and noncholinergic (right) populations. **n,** Average response to VNS for all 'activated' neurons. **o,** Mean peak activation during VNS. **p,** Average delay of peak activation from VNS onset. **q,** Mean duration of significantly elevated activity after VNS (cholinergic vs awake p=0.0087, non-cholinergic vs awake p=0.0003).

were identified by their rapid response to light (**Fig. 3h,i**) and confirmed using SALT analysis[18] (latency 5.2±1.3ms) (**Fig. 3j**). Cholinergic neurons exhibited a lower baseline firing rate (3.4±2.1hz) than the non-cholinergic population (6.8±6.2hz) (**Fig. 3k**). Of 76 units, roughly ⅓ were cholinergic (**Fig. 3l**) and half of both neuron populations were VNS responsive (52% of cholinergic, 49% of non-cholinergic; **Fig. 3m**). Of the VNS-responsive units, most cholinergic units and non-cholinergic units showed increased activity (**Fig. 3n**). This data suggests that VNS increases activity in both cholinergic and non-cholinergic populations of the BF.

A comparison of VNS-driven activation in anesthetized recordings to awake recordings suggest that the response to VNS depends on arousal state (**Fig. 3e&n**). While the peak response magnitude and timing to VNS do not change between awake and anesthetized animals (**Fig. 3o&p**), awake animals have a longer response than anesthetized animals (awake 652.7±439 ms; cholinergic: 293.7±94 ms; non-cholinergic: 235.8±127 ms; **Fig. 3q**). These results demonstrate that VNS alters BF activity during awake behavior, making it a strong candidate for mediating VNS-driven behavioral effects.

Optogenetic cholinergic inhibition prevents VNS-enhanced motor learning

Cholinergic projections are required for VNS-driven cortical map plasticity[15], but the role of cholinergic signaling in VNS-driven motor learning remains unknown. To address this gap, an inhibitory opsin (AAV-EF1a-DIO-eArch3.0-EYFP) was injected into the BF of ChAT-Cre transgenic mice, followed by implanted optical fibers and VNS cuffs (see methods) (**Fig. 4a&b**). Mice then learned to perform the skilled reach task (**Fig. 4c**). One cohort received Success VNS, a second received Success VNS paired with optical inhibition of the BF (Arch+VNS), while the control cohort was unstimulated (**Fig. 4d**). VNS animals (40.55±7.1) performed significantly better than controls (31.23±10.4), while Arch+VNS animals performed at control levels (25.59±9.3) (**Fig. 4e&f**). While all cohorts learned the task (**Fig. 4g**), cholinergic inhibition prevented VNS-driven performance increases in both the early and late (19.02±9.5) (28.66±4.1) learning phases compared to VNS mice (early: 32.81±17.1 L; late: 48.28±11.6) (**Fig. 4g**), demonstrating that phasic cholinergic signaling is necessary for VNS-enhanced motor learning.

VNS reduces off-target failures through increased reach consistency

To understand how VNS may improve reach success rates, we used a behavior apparatus (CLARA) to automate the reaching task, track forelimb kinematics in real-time, and apply VNS following automated classification of reach outcome [40] (**Fig. 5a-c**). Using video data acquired by CLARA, trials were categorized into one of four categories: success; reach failures; grasp failures; and retrieval failures (**Fig. 5d**). Success-VNS mice made fewer reach failure errors than control and Arch+VNS mice (VNS: 54.14±10.4%; control: 72.16±7.0%; Arch+VNS: 71.66±4.5%), and more on-target grasp errors (VNS: 38.19±9.2%, Arch+VNS:

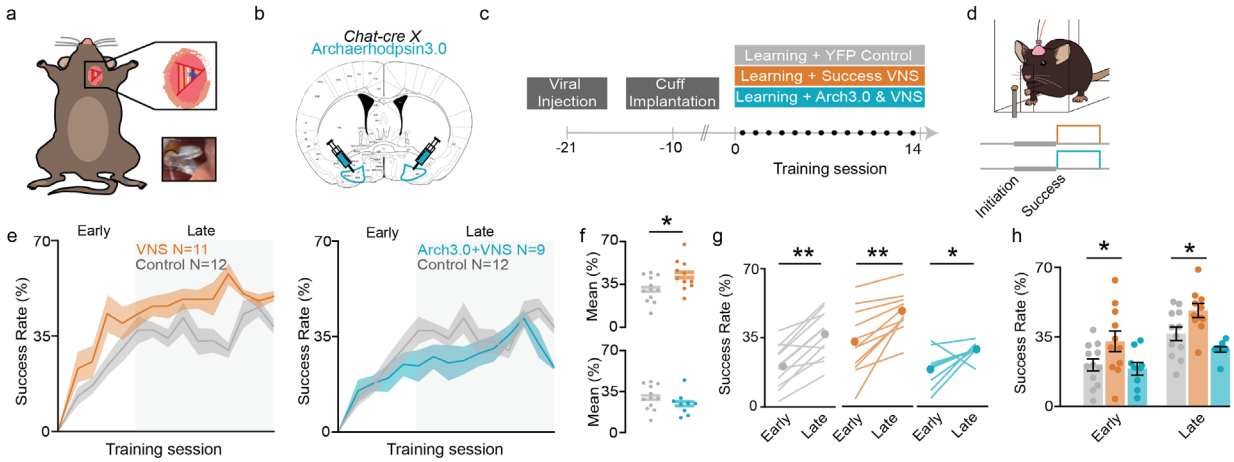

Figure 4 | Outcome-paired VNS motor learning enhancement requires cholinergic neuromodulation.
a, Schematic of VNS implant surgery. **b,** A subset of VNS-implanted *ChAT-Cre* transgenic mice also received injections of viral constructs containing Archaerhodpsin3.0 bilaterally in the BF (right). Mice were chronically implanted with bilateral fiberoptic cannulas for light delivery. **c,** Timeline of experimental set up and training. Each training session lasts for 20 minutes. **d,** Depending on cohort, mice receive VNS, or continuous 532nm light and VNS simultaneously, after successful reach attempts. **e,** Average success rate for all mice over the course of learning(VNS N=11, Arch+VNS N=9, Control N=12). **f,** Mean performance across all days between VNS and control (p=0.0409 (top)), and Arch VNS and control (p>0.05 (bottom)). **g,** Mean success rate of all groups between early and late phases (Control p=0.0001, VNS p=0.0009, Arch VNS p=0.0379). **h,** Mean success rate for control and VNS mice during early (p=0.0458) and late (p=0.0001) learning phases and control and Arch VNS mice (p>0.05).

24.00±4.8%, Control: 22.14±6.0%) (**Fig. 5e,f**). Given the reduction in 'off-target' reach failures, which implies an improved accuracy in reach trajectory, we explored if VNS drives a speed/accuracy trade-off[41]. We measured reach endpoint accuracy and outward reach velocity (see methods) (**Supplementary Fig. 3a&b**), and found that Success VNS does not alter endpoint accuracy or speed of reach attempts (**Supplementary Fig. 3c**), suggesting that it does not influence performance through modulation of either speed or endpoint accuracy.

Motor learning leads to increases in reach consistency towards an expert reach[29,42]. To determine if VNS influences reach consistency, an expert trajectory was defined for each mouse (see methods) (**Fig. 5g**) and 'expert reaches' were identified by having a >0.95 correlation with the expert trajectory. While stimulation does not alter initial reach variance (**Supplementary Fig. 3d**), VNS mice made significantly more 'expert reaches' during late learning compared to control mice (VNS: 45.22±4.4%; control: 34.22±6.6%) while Arch+VNS did not differ from controls (23.58±6.2%) (**Fig. 5i**). Expert reach attempts correlate strongly with behavioral performance (p=0.0001, r^2=0.621), demonstrating that they are a kinematic proxy to task performance (**Fig. 5h**). Likewise, in reach failures, which are not captured in the expert reach population (**Supplementary Fig. 5e**), VNS also increased the similarity of the failures to the expert trajectory during late learning as compared to control mice, while Arch+VNS mice did not differ from controls (VNS: 50.18±16.6; Control: 29.65±19.9; Arch VNS: 33.19±11.6) (**Fig. 5j**). Additional

239 kinematic features also show a VNS-driven improvement of the feature consistency between early and late
240 phases (indicated by a narrower histogram with a higher peak) (**Fig. 5k,l**). This data suggests that VNS
241 decreases off-target reach attempts through improved selection and execution of an expert trajectory late in
242 learning. Further, cholinergic inhibition prevents VNS-driven changes of kinematic features.
243
244 **VNS drives acute neural suppression and activation in motor cortex**
245 VNS paired with forelimb movement alters motor cortical map plasticity [24], but the effect of VNS on
246 neuronal function in motor cortex is unknown. Given that neural activity in mice motor cortex (M1) is
247 required for both motor skill learning and execution [42,43](**Supp. Fig. 4a**), we hypothesize that VNS will
248 modulate the neural activity and movement representation in M1. To investigate the effects of VNS in M1
249 neural activity, we first imaged neural responses to VNS in freely-moving animals expressing calcium
250 indicator GCaMP6m in M1 using a head-mounted miniature microscope in the homecage (UCLA
251 miniscope V3, http://miniscope.org, **Fig. 6a**).
252 In response to VNS, neurons demonstrated either activation (**Fig. 6b**, red, cell 25) or suppression (**Fig. 6b**,
253 blue, cell 36), without a change in the overall firing rate of the neuron population (**Supp. Fig. 5a&b**).
254 Approximately 30% of all neurons showed acute response to a VNS delivery, with roughly similar
255 percentages of neurons showing activation and suppression (activation: 13.8 ± 5.8%; suppression: 18.1 ±
256 15.8%; **Fig. 6d**), and only a small fraction (0.7 ± 1.4%) show bidirectional modulation (**Fig. 6d**). The
257 number of neurons modulated by VNS showed a dose-dependence on stimulation intensity (**Fig. 6e**).
258 We next investigated the temporal dynamics of VNS activation and suppression (**Fig. 6c,f**). The
259 mean peak timing of the suppression precedes the activation by 1.2s (**Fig. 6g**; suppression: 1.6 s from VNS
260 onset; activation: 2.8 s), a relationship consistent across a range of behaviorally relevant stimulation

261

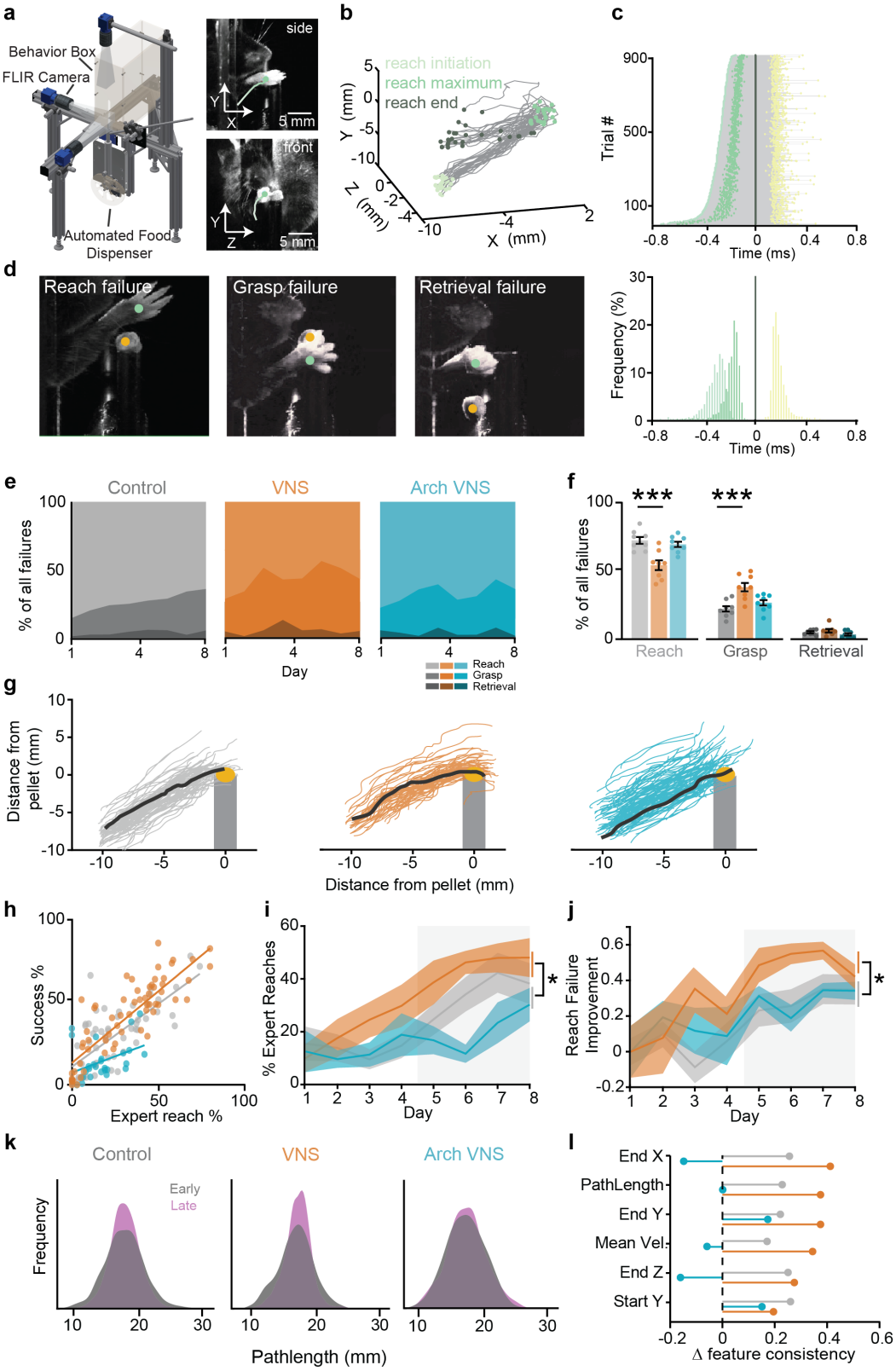

Figure 5 | VNS improves performance through improved consolidation of reach trajectory.
a, The Closed-loop automated reaching apparatus (CLARA) provides 3D tracking of the paw and pellet. **b**, A custom CLARA data pipeline automatically identifies reaching events (one mouse one control session). **c**, CLARA rapidly delivers stimulation after reach end in a closed-loop fashion (180±5ms). Top: duration of all stimulated control trials, yellow dot denotes stimulus delivery. Bottom: a histogram of reach timepoints normalized to reach end.

intensities (**Fig. 6h**). Similarly, the onset of suppression preceding activation by 0.6 seconds (**Supp. Fig. 5c**). These together suggest that in the forelimb region of the mouse primary motor cortex, VNS first drives acute neural suppression, followed by activation in a subpopulation of neurons without altering the mean population firing rate.

Success VNS modifies the task-related neural representation of the skilled reach during learning

We examined the influence of Success VNS on movement representation during early learning. The neural activity in M1 of freely-moving mice implanted with VNS cuff and trained to reach in CLARA was measured by imaging GCaMP6m in neurons with a head-mounted miniscope. Each reach was subdivided into a reach and an outcome phase using post hoc analysis (**Fig 7a**). The reach phase includes the outward paw movement from reach initiation to reach max (~100 ms) and the return movement from reach max to reach end (to 200 ms). Reach outcome (success or failure) is typically detected to 350 ms after reach max and ~200ms after reach end. As anticipated [44–47], the average population activity is significantly modulated during movement (either the reach or outcome phase; **Fig. 7b**). Nearly half of all neurons were movement modulated (44% of all neurons), with 13.3% of all neurons modulated during reach and 31.7% modulated during success outcome. For success-outcome-modulated neurons, roughly half are activated and half suppressed (**Fig. 7c**, success-activated: 16.3 ± 6.4%; success-suppressed: 15.4 ±10.2%). The outcome representation of success differs from failure, both at the level of the population average response (**Supp. Fig. 6 a&b**) and individual neural responses (**Supp. Fig. 6 c&d**).

During Success VNS, stimulation is delivered at reach outcome, and so the acute neural response to VNS is likely to overlap with the intrinsic response to success outcome. To accurately detect VNS-related neural activity, mice participated in two sessions of training, one with VNS and one without, administered on a pseudo-randomized schedule (**Fig. 7d**), and the average neural response was compared between VNS and no-stimulation sessions. During VNS sessions, the success-activated neurons' average response was first attenuated, then slightly enhanced (**Fig. 7e**). In contrast, success-suppressed (**Fig. 7f**), nonmodulated

Figure 5 | VNS improves performance through improved consolidation of reach trajectory (con't).
d, Example images of the three subcategories of failed reaches (see METHODS). **e**, Breakdown of failure outcomes for each group over 8 days of learning. Light colors: reach failures; intermediate : grasp failures; dark: retrieval failures. **f**, A comparison of types of failed attempts between control and VNS (reach errors: p=0.0005; grasp errors: p=0.0035) and between control and Arch+VNS mice (p>0.05) (VNS N=8, Arch+VNS N=8, Control N=8). **g**, Examples of all outward trajectories (reach initiation – reach maximum) during a session on day 8. Black lines represent each mouse's 'expert reach'. **h**, Correlation of 'expert' reaches and task performance for all mice, r^2=0.62. i, Percent of reaches that are 'expert'. Comparisons were made for the mean 'expert' reaches in the late learning phase (grey box) between control and VNS mice (p=0.0142) and control and Arch+VNS mice (p>0.05) (VNS N=8, Arch+VNS N=6, Control N=8). **j**, Percent of improvement in 'reach failure' toward expert trajectory as measured by increase in correlation coefficient. Comparisons were made during late learning between control and VNS mice (p=0.0455) and control and Arch+VNS mice (p>0.05). **k**, Distribution of trajectory lengths from all failure attempts during early (grey) and late (purple) learning phases. **l**, Normalized improvement in reach features from early to late learning phases.

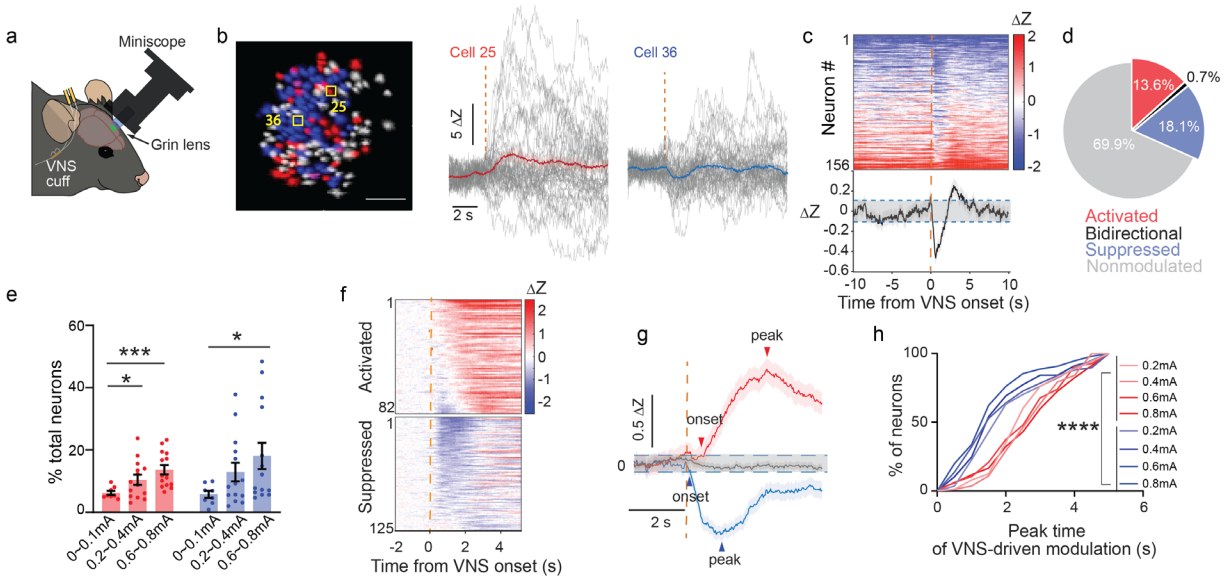

Figure 6 | VNS drives acute neural suppression and activation in forelimb motor cortex
a, Placement of the grin lens and miniscope above contralateral M1, VNS cuff in the neck and its wire connectors on top back of skull. **b,** Left, representative neural ROIs from one mouse M1 (n = 156 neurons): VNS-activated (red) and suppressed (blue), scale bar = 100 µm. Middle and right: two representative neurons' responses aligned by VNS onset (gray: individual trials; red: VNS-activated; blue: VNS-suppressed). **c,** Top: individual neurons' average responses z-scored to inactive phases of all neurons from the representative mouse in **b**; bottom: average neural responses of all neurons from the same mouse. **d,** Average % of total neurons response after 0.6 to 0.8mA VNS delivery (N = 7 mice, 767 neurons). **e,** % of total neurons that are activated or suppressed by VNS across different current amplitudes. (N = 7 mice, n= 747 to 807 total neurons from each stimulation group, One-way ANOVA and multiple group comparison to 0 to 0.1 mA group, * $p < 0.05$, ** $p < 0.01$, *** $p < 0.001$). **f,** Neural response of all activated and suppressed neurons. **g,** Average neural activity of all activated and suppressed neurons aligned at VNS onset (N=7 mice, 82 activated neurons, 125 suppressed neurons, 0.6mA VNS). **h,** Cumulative distribution of neural response peak time of activated and suppressed neurons measured as the peak value of the average trace 0 to 5 seconds after VNS onset (82 to 151 neurons from each group, Kruskal-Wallis test followed by Dunn's multiple comparisons test, $p < 0.0001$).

population response (**Fig. 7e**), nearly half of individual neuronal responses were enhanced by VNS (43.3%; **Fig. 7i,k**) and a similar portion were attenuated (40.9%; **Fig. 7j, k**). We next considered if attenuated neural responses preceded the enhanced responses, similar to the temporal dynamics of activation and suppression in the homecage (**Fig. 6g, h**). Indeed, the peak attenuation occurs with similar latency to homecage VNS suppression (1.85 ± 1.20s vs. 1.78 ± 1.10s; **Supp. Fig. 6g**), followed by peak enhancement at a similar latency to peak activation in the homecage context (2.65±1.50s vs.2.74±1.20s, **Supp. Fig. 6g**), demonstrating a similar temporal structure to the VNS response both during and outside of the reach behavior.

Having established that many success-activated neurons are acutely modulated by VNS during success outcome, we next wanted to explore if this neuronal population displays additional activity differences during other phases of the reach. To measure activity across the reach, neural activity was compared to a pre-reach baseline epoch, and differences between the reach representation were compared between the Success VNS and no-stimulation sessions (**Fig. 7l**). Approximately 60% of success-activated VNS-modulated neurons show activity differences onset prior to VNS (**Fig. 7m**). More broadly, during the

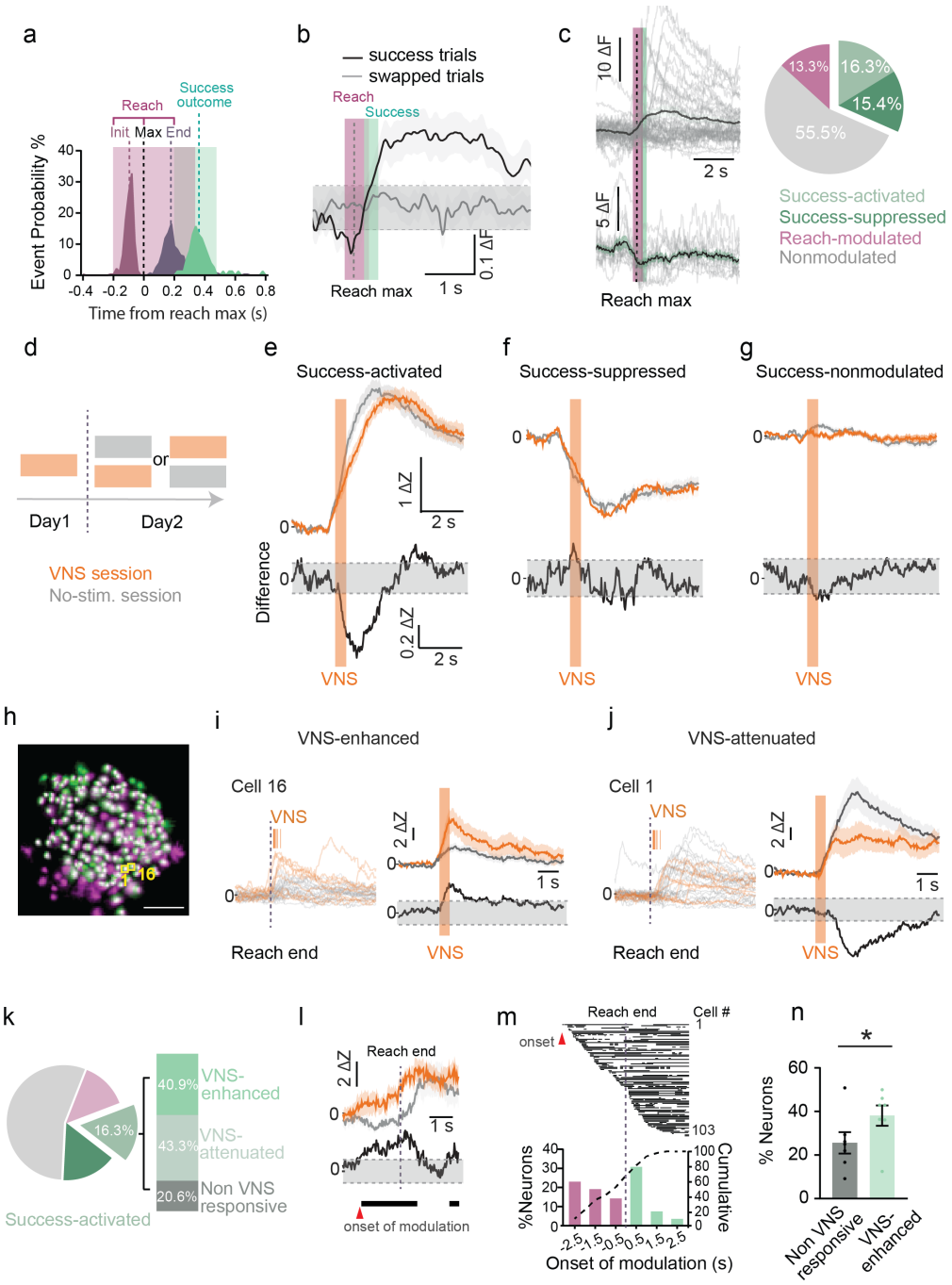

Figure 7 | Success VNS selectively modulates activity of task-activated M1 neurons in the reach task.
a, Peri-event histogram of the task related events aligned at reach max (n = 6 control mice, day 4, n = 278 single-reach success trials). Dashed lines indicate median reach initiation (-93 ms), reach max (0 s), reach end (180 ms) and outcome recognition (360 ms). **b**, Average neural activity of success trials (black) and random control trials (grey, n = 488 neurons). Gray dashed line indicates 2 s.d. from the baseline mean. c, Left: representative neural responses: red success-activated, blue success-suppressed, gray individual trials. Right: % neurons modulated in the task (903 neurons). **d**, Assignment of VNS or no-stimulation sessions. **e-g**, Top: Average responses of success-activated (d,115 and 101 neurons), success-suppressed (e, 122 and 92 neurons) and success-nonmodulated neurons (f, 383 and 394 neurons) in VNS (orange) and in no-stimulation session (gray). Bottom: the difference trace. **h**, Registered neurons (white) in VNS (green) and no-stimulation session (Magenta). **i&j**, Left: single trial responses in no-stimulation session and in VNS session (orange ticks: VNS onset). Right: the average and difference responses of the same neurons aligned by VNS onset. **k**, Percentage of success-activated neurons (n = 77 registered) that are enhanced (40.9 ± 13.7%) or attenuated (43.3 ± 21.2%) in VNS compared to no-stimulation session. **l**, One success-activated neuron modulated by VNS. Arrowhead: onset of increased activity. **m**, Onset of VNS-driven modulation. **n,** % neurons modulated in reach in VNS-nonmodulated versus VNS-enhanced neurons.

VNS session, all VNS-enhanced neurons are more likely to be active during the reach phase than non-VNS modulated neurons (38.1 ± 4.7% vs. 25.6 ± 4.9%; **Fig. 7n**). Since VNS alters neural response during the entire reaching movement, this suggests that VNS effects persist beyond the initial acute modulation during outcome.

VNS-driven acute neural modulation is mediated through acetylcholine receptors (AChR)

To determine if the acute effects of VNS on neural activity in M1 are mediated through cholinergic signaling, we injected a systemic acetylcholine receptor antagonist cocktail and measured the acute neural response to VNS in M1 in the awake, freely-moving animal. The baseline acute VNS response in M1 was first measured in homecage, then 15 minutes following administration of AChR antagonist cocktail, and finally in a washout session ~24 hours later (**Fig. 8a**). The percentage of the VNS-modulated neural population was not changed by AChR antagonism (supp. **Fig. 7**). However, the response amplitudes of VNS modulated neurons, both activated and suppressed, were reduced by cholinergic antagonism (**Fig. 8b-e**), demonstrating that AChR mediated signaling is required for VNS-driven acute neural activation and suppression.

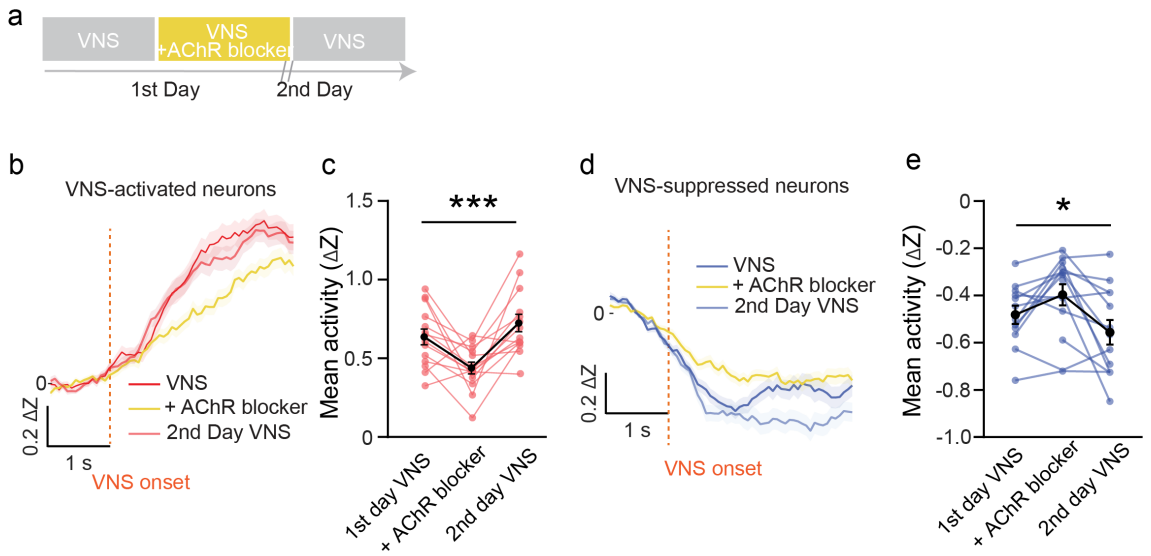

Figure 8 | VNS driven acute neural modulation is mediated through AChRs.
a, Diagram of experimental design: three sessions including a control VNS session in home cage, VNS session with AChR blocker, recovery VNS session on the 2nd day. **b&d,** Average neural activity of VNS-activated neurons (**b,** n = 104 ~116 neurons) or VNS-suppressed neurons (**d,** n = 124~143 neurons) in control VNS session, VNS session with AchR blocker and the 2nd day recovery VNS session. **c,** Average neural activity comparison of VNS-activated neurons quantified from 0.8 to 2.8 seconds after VNS onset, defined based onset and peak delay of VNS-driven neural activation in Figure. 6 (N = 7 mice x two repeats each mouse, Repeated measures ANOVA, $p < 0.001$). **e,** Average neural activities comparison of VNS suppressed-neurons quantified from 0.2 to 1.6 seconds from VNS onset defined based onset and peak delay of VNS-driven neural suppression in Figure. 6 (N = 7 mice x two repeats each mouse, Repeated measures ANOVA, $p = 0.02$,).

Discussion

Vagus nerve stimulation paired with rehabilitation is proposed as therapeutic treatment for a wide range of neurologic conditions, yet the mechanism by which VNS may drive neuronal activity to produce changes in behavior remains relatively unexplored. In this study, we establish that VNS optimally enhances motor learning when paired with reach success. VNS drives activity of cholinergic neurons in BF, and optogenetic inhibition of cholinergic neurons is sufficient to eliminate the effects of paired VNS on motor learning, and to reverse VNS-driven kinematic improvements of the reach. Longitudinal in vivo imaging of neurons of the primary motor cortex shows that VNS selectively modulates neurons that represent reach outcome, suggesting a mechanism by which VNS influences reinforcement cues. The effects of VNS on M1 neural activity depend on cholinergic signaling. Together, these results demonstrate that paired-VNS accelerates motor learning through reinforcement, mediated by cholinergic-dependent changes in neural representation and reach kinematics.

VNS paired with reach success optimally enhances motor learning

To our knowledge, we are the first to demonstrate the importance of pairing VNS to movement outcome to enhance motor learning. VNS induces cortical map plasticity in healthy animals when paired with specific movements[24] or auditory tones[48] but has not been shown to improve task performance [24,49]. In contrast, we find that VNS paired with a successful reach, but not reach initiation, enhanced motor learning and ultimate performance. The enhanced motor learning may be due to the pairing of VNS stimulation with a successful task outcome, perhaps to augment task reward or reinforcement. Endogenous activity of the vagal nerve has been linked to reward and motivation[50], and VNS in human subjects drives motivation towards reward [51] and improves reinforcement learning[52]. However, VNS does not seem to activate classical dopaminergic reward pathway [32] as conditioned place preference test results indicate that VNS is not inherently rewarding of aversive. Instead, VNS may augment reinforcement cues, leading to improved selection of successful trajectory[53,54] and the associated neural ensembles that underlie those movements[55–57]. By augmenting reinforcement cues, VNS may help to select the appropriate neural circuits, strengthening those connections for lasting improvements in functional outcome.

The importance of VNS timing appears to differ across the learning process. During early learning, Success VNS has a unique ability to improve reach learning. Moreover, Random VNS delivered during early learning impairs reach learning, suggesting that poorly timed VNS can disrupt normal learning processes. During late learning, Success VNS maintains improved performance over control animals, while the subset of stimulated trials in Reach VNS also show performance improvements over controls (but this improvement is abolished when all trials are included). In expert animals, both Success and Reach VNS provide short-term improvements over unstimulated blocks of trials. Thus, it appears critical that VNS be

paired with reach outcome during early learning, but there is more flexibility in the timing of VNS pairing during the rehearsal of a known task.

How might reinforcement-paired VNS contribute to skilled motor learning? Motor learning travels along an exploration-exploitation axis, with early exploration, expressed as motor variability, reducing as the motor behavior consolidates onto an expert solution [58–60]. Moreover, early learning motor variability predicts improved later performance of the expert motor solution [54,61,62], pointing to a reinforcement learning process by which increased exploration allows for faster identification of the expert solution. Reward is also known to influence the exploration-exploitation relationship, with conditions of increased reward frequency leading to reduced variability and increased consolidation onto a motor solution [53,60,63]. Our results show that paired-VNS does not increase variability in early learning, but instead improves kinematic consolidation onto an expert reach. Perhaps, in this context, VNS acts to reinforce the reward salience, increasing the exploitation of the expert solution. Future experiments are needed to explore if VNS can reinforce movements in the without association to a food reward.

VNS-driven motor learning is mediated by cholinergic signaling

VNS activates multiple neuromodulatory systems in the central nervous system[16,64,65], and the effects of VNS on cortical plasticity are mitigated with lesions of neuromodulatory nuclei including the locus coeruleus, raphe nucleus and the cholinergic basal forebrain[15,16]. While each of these neuromodulators could play a role in motor learning, cholinergic neuromodulatory systems are critical for use-dependent plasticity[34,66–69], are most closely associated with reinforcement signaling[18,33], and encode task outcome[19,70]. Lesions[17,71] or pharmacological suppression of cholinergic neurons[72] are detrimental to motor learning and VNS-enhanced motor rehabilitation[9]. Leveraging the temporal precision of optogenetic suppression of cholinergic neurons, we find that a brief cholinergic inhibition is sufficient to prevent VNS-driven enhancement in motor learning. This suggests that the effects of Success VNS are mediated through cholinergic signaling in the basal forebrain, and is consistent with the role of the cholinergic BF to encode outcome salience[18,19,70].

Only limited evidence exists demonstrating an anatomical or functional connection between the vagus nerve and the cholinergic basal forebrain[73]. Using optotagging approaches, we were able to demonstrate robust functional connectivity between the BF and the vagus nerve. Stimulation of the vagus nerve elicited robust responses in nearly half of the cholinergic and non-cholinergic units recorded under anesthesia and more than 40% of the units recorded in awake animals. The variable timing of BF neuronal responses to VNS suggests the involvement of a multi-synaptic pathway, possibly through the locus coeruleus (LC), which is known to send direct projections to the BF[74–76] and is activated by VNS[13,77].

Additionally, VNS leads to the sequential activation of noradrenergic and cholinergic axons in cortex, with noradrenergic activity preceding cholinergic activity[14].

Motor cortical neurons are modulated by VNS via cholinergic activity

Neurons in the primary motor cortex represent movement preparation and execution for dexterous movements [43,78,79]. During motor learning, these neural representations are updated to improve motor output [46,80,81] by incorporating feedback from error and reinforcement signals generated throughout multiple regions of the central nervous system, including cortical regions [55,82–84]. Recent work demonstrated that, in addition to movement preparation and execution, primary motor cortex (M1) pyramidal neurons also report movement outcome. Neurons in superficial L2/3 of M1 represent success and failure, independent of kinematics and the food reward consumption [47]. Our data demonstrate that Success VNS attenuates the population representation of a success outcome by selectively modulating success-outcome responsive neurons. This same neural population is also more likely to have different representation of movement preparation and reach execution as well, suggesting that VNS changes neural activity beyond the acute response to stimulation. The specificity of the population of neurons that are modulated by Success VNS may indicate that VNS adds selectivity to outcome representation, to optimize outcome signals for enhanced learning.

The relative selectivity of the effects of Success VNS on movement representation are somewhat in contrast to recent observations of widespread, long-lasting excitatory responses to VNS [14]. However, in the previous study, in head-fixed mice VNS elicited locomotion and whisking, both of which correlate to increased general arousal and widespread cortical activation [85–87], making it difficult to disentangle direct VNS effects from changes in arousal. In contrast, another recent work demonstrated a VNS-driven suppression of neural response to an auditory tone that persisted even after arousal state was regressed from the neural response [88]. Our trial design controls for movement state, as the comparison between the VNS trial and no-stimulation trial occurs at the exact same reach position, and VNS did not produce any noticeable acute motor response. By eliminating the confound of behavioral states such as locomotion or quiet resting, we can detect that VNS produces an initial suppression of the outcome response followed by excitation. This effect is seen only in neurons that respond to outcome, indicating that when applied during a reach, VNS acts on a specific population of neurons that are already engaged in the representation of reach outcome.

Mechanisms of other neurotechnology during motor learning and performance

Motor learning and performance have been modulated utilizing non-invasive stimulation devices including transcranial stimulation (ie. tCDS, TRMS) and transcranial magnetic stimulation (TMS). While both tCDS

428 and TMS have relatively unknown mechanisms, they are postulated to operate by inducing polarity changes
429 in cortical neurons altering their excitability[89–91] and promote BDNF-mediated synaptic plasticity[92]. Still,
430 the underlying mechanisms and optimal stimulation protocols are a current area of exploration[93]. For
431 example, some tCDS studies have shown improved reaction times in motor sequence tasks[89,94], yet others
432 have reported no effect on reaction time or performance [95,96]. As with VNS, further exploration of the
433 mechanisms of action of non-invasive stimulation modalities, along with optimized stimulation protocols,
434 is needed to address specific therapeutic needs across a wide range of neurologic disorders.
435
436 **Conclusion**
437 In conclusion, we demonstrated that VNS augments reinforcement cues to accelerate skilled motor learning
438 and enhance kinematic consolidation on an optimal motor plan in healthy animals. VNS alters neural coding
439 of outcome in a select neural population, and changes neuronal activity of this population across the entire
440 reach. The behavioral, kinematic and motor representation effects of VNS are mediated by phasic
441 cholinergic activity. Understanding the behavioral and circuit mechanisms of VNS allows for future
442 optimization of rehabilitation protocols and new avenues for the use of cholinergic manipulation to treat
443 neurologic conditions.
444
445

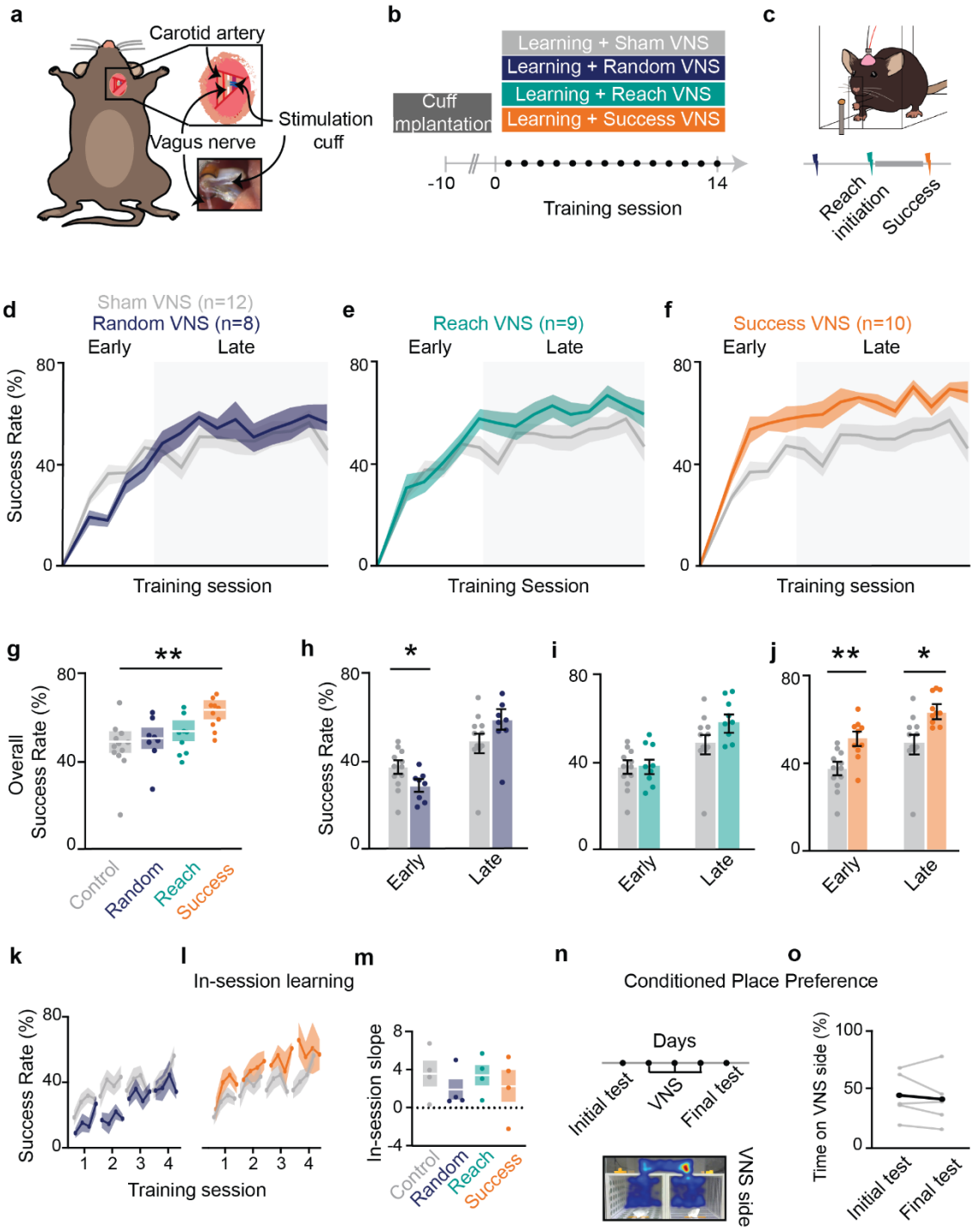

Figure 1 | VNS modulates forelimb reach learning and requires temporally specific stimulation. a-c, Illustration of VNS surgery, behavior timeline, and stimulation protocol. **d-f,** Random VNS, Reach VNS,

and Success VNS success rate across 14 sessions of training. **g,** Comparison of mean performance across all days between control and stimulated groups (Success VNS: $p=0.0065$, $f=9.24$, Random VNS: $p>0.05$, Reach VNS: $p>0.05$, Student T test). **h,** Comparison of mean success rate for control and Random VNS mice during early ($p=0.028$, $f=7.07$, Student T test) and late learning ($p>0.05$). **i,** Comparison of mean success rate for control and Reach VNS mice during early and late learning ($p>0.05$). **j,** Comparison of mean success rate for control and Success VNS mice during early ($p=0.0031$) and late learning ($p=0.0126$). **k,l,** in-session learning trajectories for each group. **m,** Comparison of within session learning between all groups across 4 days of learning. **n, o,** VNS mice performed a conditioned place preference test after 3 days being stimulated in one of two distinct rooms. $*p < 0.05$, $**p < 0.01$, $***p < 0.001$ bars and error bars represent the mean ± s.e.m.

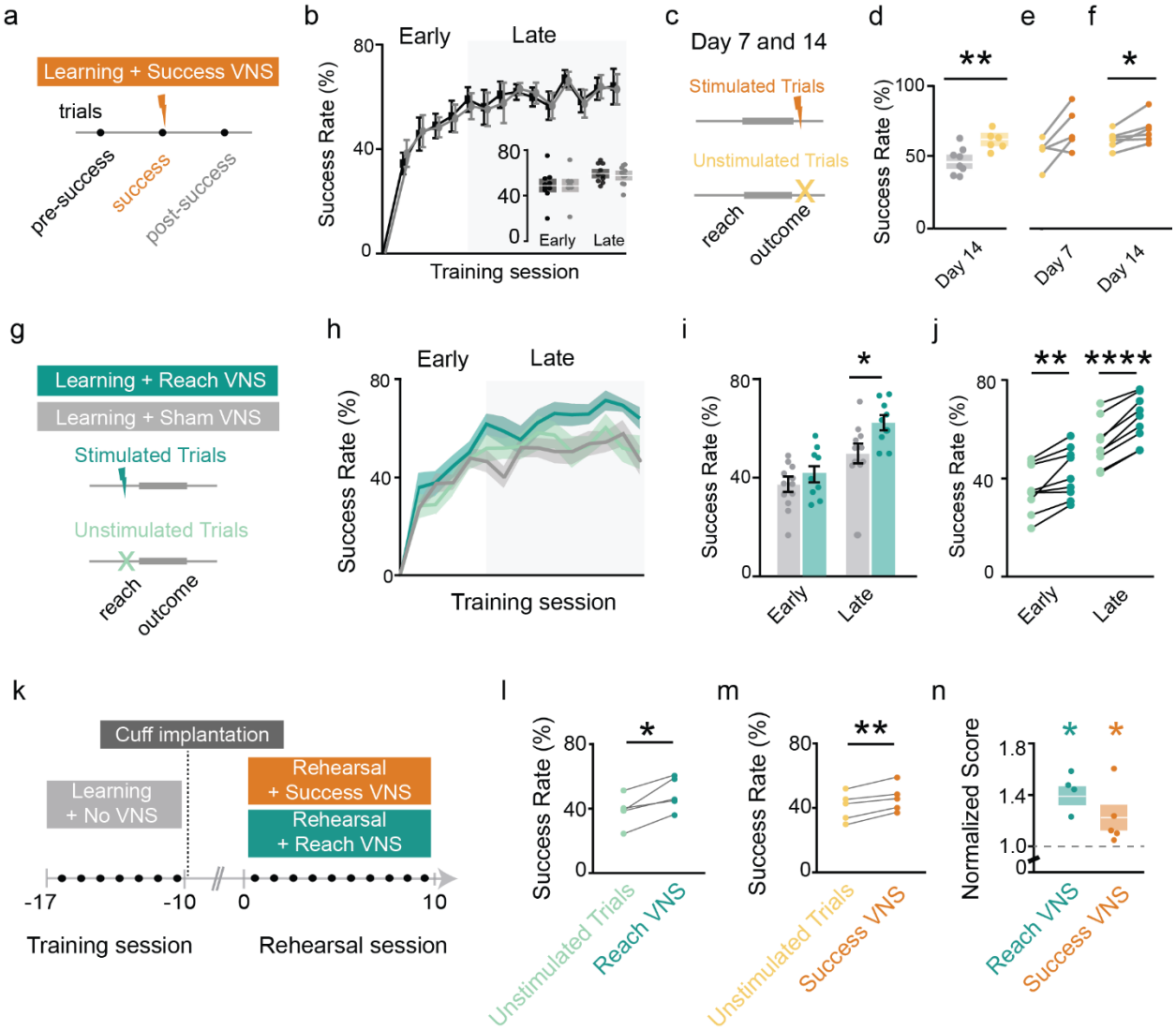

Figure 2 | VNS improves success rate within sessions and in learned mouse during rehearsal of forelimb reach task. a, trials before and after a stimulated success are investigated in success VNS **b,** Comparison of success rate for reaches preceding or following stimulated reach. **c,** For Success VNS, day 7 and 14 trials are divided into equal blocks of unstimulated and stimulated trials. **d,** Comparison of unstimulated (light orange) and sham (grey) trials on day 14 (p=0.0059, t=3.34, Student's T test). **e&f,** Comparison of stimulated (dark orange) and unstimulated (light orange) trials on days 7 & 14 (Day 7: p>0.05; Day 14: p=0.0499, t=2.57, Ratio paired t test). **g,** Reach VNS schematic **h,** Success rates across learning training sessions for Sham (grey), Stimulated Reach VNS (dark green), and Unstimulated Reach VNS (light green). **i,** Comparison of stimulated Reach VNS and Sham VNS trials in early (p>0,05) and late learning (p=0.024, t=2.47, Student's T test). **j,** Comparison between stimulated Reach VNS and unstimulated Reach VNS trails in early (p=0.004, t=3.98, paired t test) and late learning (p<0.0001, t=10.08,

475 paired t test). **k,** Success VNS and Reach VNS applied during rehearsal of reach task in naively trained
476 mice. **l,** Stimulated Reach VNS trials improve success rate during rehearsal ($p=0.015$, $t=4.058$, paired t
477 test). **m,** Stimulated Success VNS trials improve success rate during rehearsal ($p=0.005$, $t=5.62$, paired t
478 test). **n,** Normalized improvement of stimulated Reach VNS ($p=0.047$, $t=3.56$) and stimulated Success VNS
479 trials ($p=0.028$, $t=4.16$) compared to unstimulated trials (Sidak's multiple comparison's test in RM one-
480 way ANOVA). $*p < 0.05$, $**p < 0.01$, $***p < 0.001$; bars and error bars represent the mean ± s.e.m.
481
482

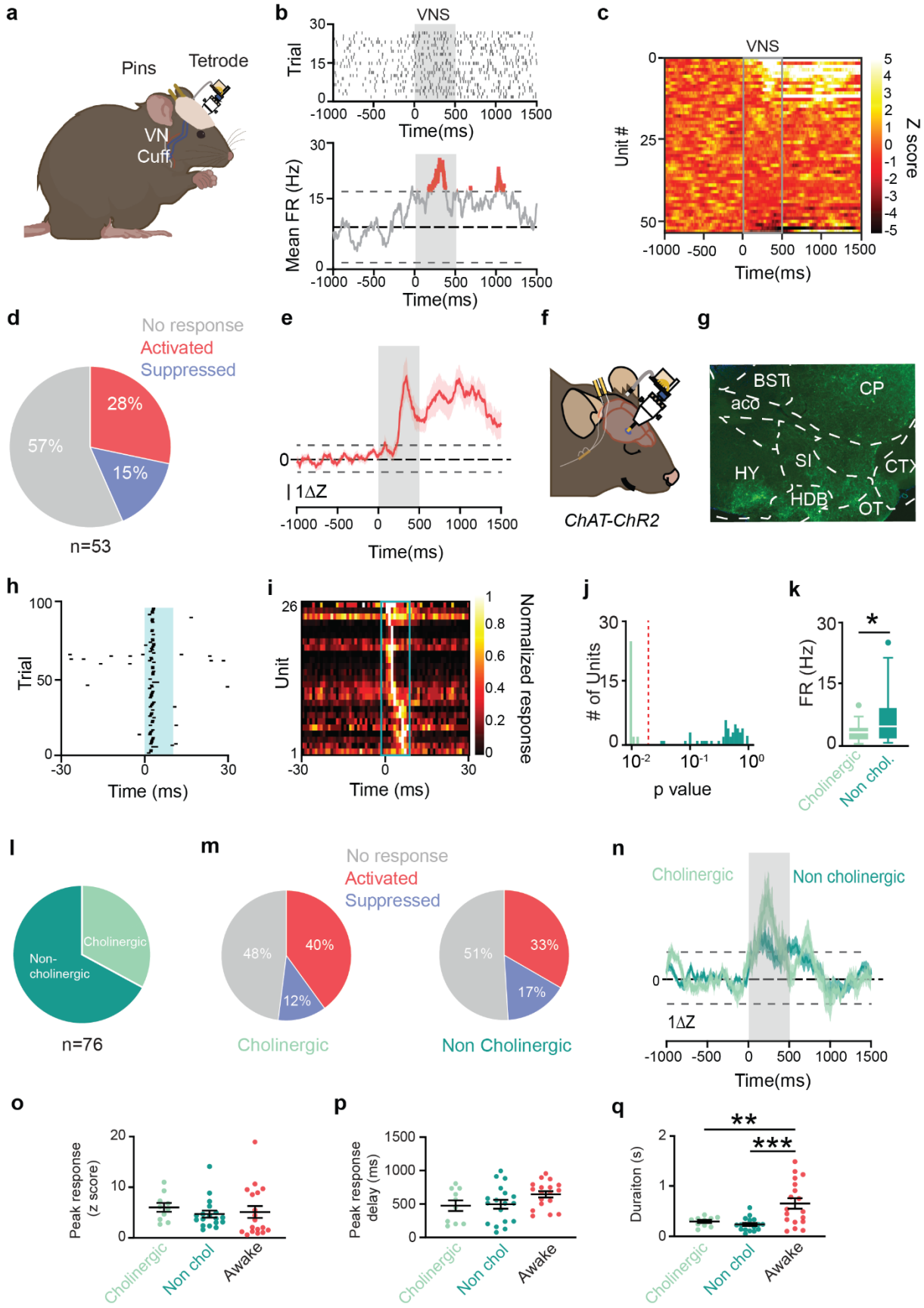
a
Pins
Tetrode
VN
Cuff
b
VNS
Trial
Time(ms)
Mean FR (Hz)
c
VNS
Unit #
Z score
Time(ms)
d
No response
Activated
Suppressed
28%
57%
15%
n=53
e
1ΔZ
Time(ms)
f
ChAT-ChR2
g
BSTi
CP
aco
SI
HY
CTX
HDB
OT
h
Trial
Time (ms)
i
Unit
Normalized response
Time (ms)
j
# of Units
p value
k
FR (Hz)
*
Cholinergic
Non chol.
l
Cholinergic
Non-cholinergic
n=76
m
No response
Activated
Suppressed
48%
40%
12%
Cholinergic
51%
33%
17%
Non Cholinergic
n
Cholinergic
Non cholinergic
1ΔZ
Time(ms)
o
Peak response (z score)
Cholinergic
Non chol
Awake
p
Peak response delay (ms)
Cholinergic
Non chol
Awake
q
**
***
Duraiton (s)
Cholinergic
Non chol
Awake

Figure 3 | VNS drives BF neural activity in anesthetized and awake mice.

a, Tetrodes were implanted in the left BF of mice and recordings were obtained during awake behavior. **b,** Example raster (top) and average firing rate (bottom from an 'activated' neuron) in response to VNS. Grey box denotes stimulus delivery. **c,** Heatmap showing the average responses of all recorded neurons to VNS (grey box). White represents increased activity; black represents decreased activity. **d,** Percent of neurons that respond to VNS (N = 5 mice, 53 neurons). **e,** Average activity of all 'activated' neurons in response to VNS. Dashed lines mark significantly altered activity, shading represents SE. **f,** Extracellular recordings were obtained using optrodes while under light anesthesia. **g,** Optrodes were targeted at the HDB in *ChAT-ChR2* transgenic mice. Green fluorescence denotes the presence of ChR2. **h,** Example cholinergic neuron responding consistently to pulses of 488 nm light. **i,** Average activity of all cholinergic neurons during opto-tagging. Each row represents a neuron. **j,** Stimulus-associated latency tests (SALT) separate light responsive neurons from non-light responsive neurons. **k,** Mean baseline FR of cholinergic and non-cholinergic neurons (p=0.013, N = 5 mice, 53 neurons). **l,** Percent of neurons categorized as cholinergic (light green) and non-cholinergic (dark green) (N = 6 mice, 76 neurons). **m,** Percent of units that are VNS-responsive in cholinergic (left) and noncholinergic (right) populations. **n,** Average response to VNS for all 'activated' neurons. **o,** Mean peak activation during VNS in cholinergic, non-cholinergic and awake-recorded(red) neurons. **p,** Average delay of peak activation from VNS onset cholinergic, non-cholinergic and awake-recorded(red) neurons. **q,** Mean duration of significantly elevated activity after VNS (cholinergic vs awake p=0.0087, non-cholinergic vs awake p=0.0003).

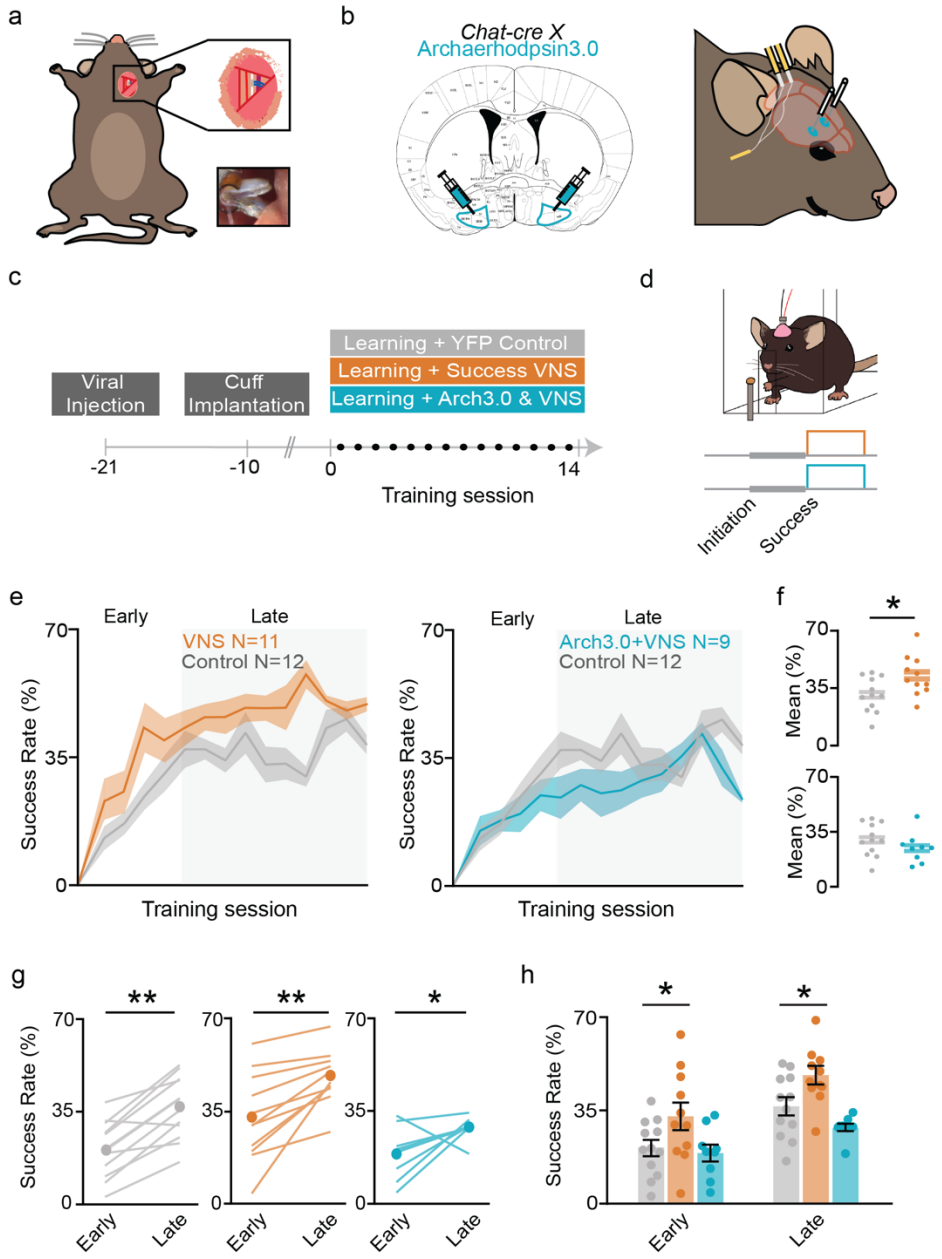

Figure 4 | Outcome-paired VNS motor learning enhancement requires cholinergic neuromodulation. **a,** Schematic of VNS implant surgery. **b,** A subset of VNS-implanted *ChAT-Cre* transgenic mice also received injections of viral constructs containing Archaerhodpsin3.0 bilaterally in the BF (right). Mice were chronically implanted with bilateral fiberoptic cannulas for light delivery (left). **c,** Timeline of experimental set up and training. Each training session lasts for 20 minutes. **d,** Depending on cohort, mice receive VNS, or continuous 532nm light and VNS simultaneously, after successful reach attempts. **e,** Average success rate for all mice over the course of learning (VNS N=11, Arch+VNS N=9, Control N=12). **f,** Comparison of mean performance across all days between VNS and control (p=0.0409 (top)), and Arch VNS and control

515 (p>0.05 (bottom)). **g,** Comparison of mean success rate of all groups between early and late phases (Control
516 p=0.0001, VNS p=0.0009, Arch VNS p=0.0379). H). Comparison of mean success rate for control and
517 VNS mice during early (p=0.0458) and late (p=0.0001) learning phases and control and Arch VNS mice
518 (p>0.05).
519
520

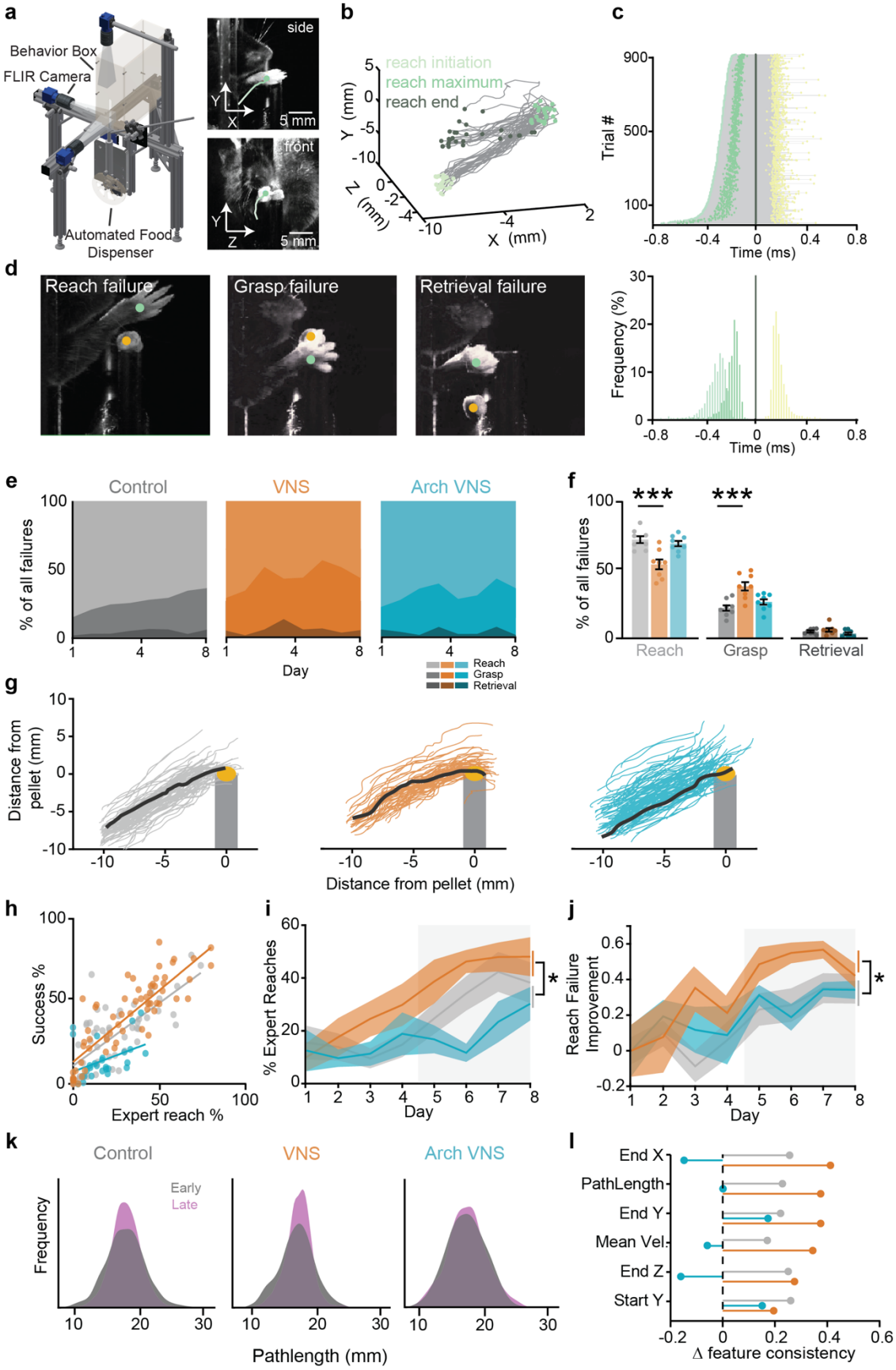
a
Behavior Box
FLIR Camera
Automated Food Dispenser
side
front
5 mm
b
reach initiation
reach maximum
reach end
Y (mm)
Z (mm)
X (mm)
c
Trial #
Time (ms)
d
Reach failure
Grasp failure
Retrieval failure
Frequency (%)
Time (ms)
e
Control
VNS
Arch VNS
% of all failures
Day
Reach
Grasp
Retrieval
f
% of all failures
Reach
Grasp
Retrieval
g
Distance from pellet (mm)
Distance from pellet (mm)
h
Success %
Expert reach %
i
% Expert Reaches
Day
j
Reach Failure Improvement
Day
k
Control
VNS
Arch VNS
Early
Late
Frequency
Pathlength (mm)
l
End X
PathLength
End Y
Mean Vel.
End Z
Start Y
Δ feature consistency

Figure 5 | VNS improves performance through improved consolidation of reach trajectory.

a, The Closed-loop automated reaching apparatus (CLARA) provides 3D tracking of the paw and pellet. **b**, A custom CLARA data pipeline automatically identifies reaching events (one mouse one control session). **c**, CLARA rapidly delivers stimulation after reach end in a closed-loop fashion (180±5ms). Top: duration of all stimulated control trials, yellow dot denotes stimulus delivery. Bottom: a histogram of reach timepoints normalized to reach end. **d**, Example images of the three subcategories of failed reaches (see METHODS). **e**, Breakdown of failure outcomes for each group over 8 days of learning. Light colors: reach failures; intermediate: grasp failures; dark: retrieval failures. **f**, A comparison of types of failed attempts between control and VNS (reach errors: $p=0.0005$; grasp errors: $p=0.0035$) and between control and Arch+VNS mice ($p>0.05$) (VNS N=8, Arch+VNS N=8, Control N=8). **g**, Examples of all outward trajectories (reach initiation – reach maximum) during a session on day 8. Black lines represent each mouse's 'expert reach'. **h**, Correlation of 'expert' reaches and task performance for all mice, $r^2=0.62$. i, Percent of reaches that are 'expert'. Comparisons were made for the mean 'expert' reaches in the late learning phase (grey box) between control and VNS mice ($p=0.0142$) and control and Arch+VNS mice ($p>0.05$) (VNS N=8, Arch+VNS N=6, Control N=8). **j**, Percent of improvement in 'reach failure' toward expert trajectory as measured by increase in correlation coefficient. Comparisons were made during late learning between control and VNS mice ($p=0.0455$) and control and Arch+VNS mice ($p>0.05$). **k**, Distribution of trajectory lengths from all failure attempts during early (grey) and late (purple) learning phases. **l**, Normalized improvement in reach features from early to late learning phases.

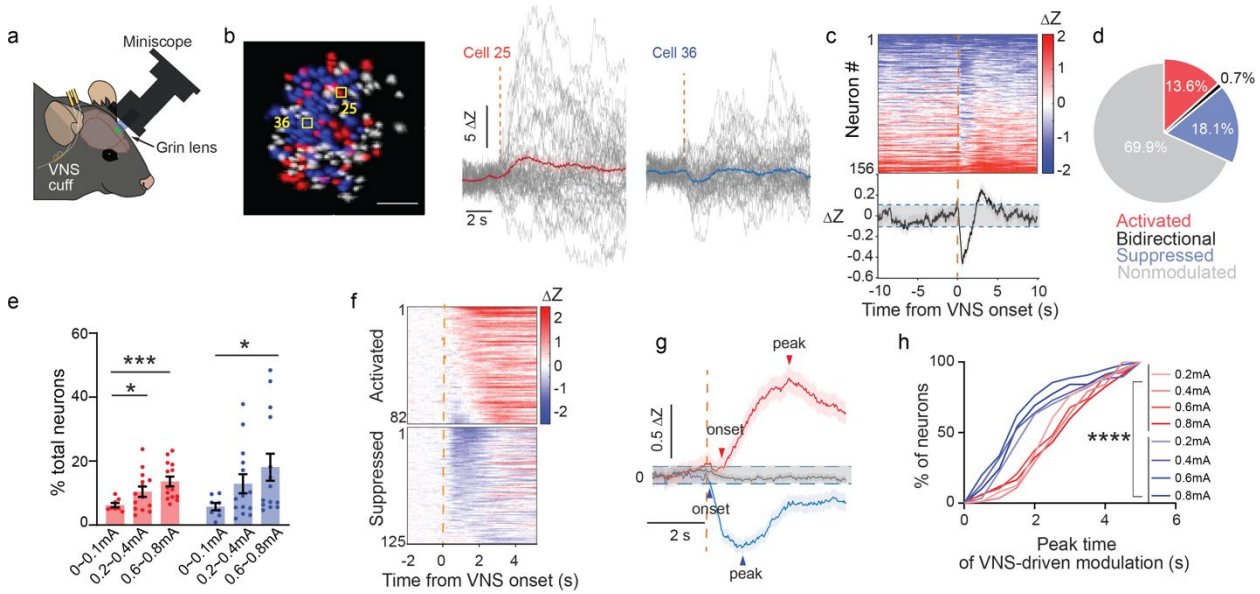

Figure 6 | VNS drives acute neural suppression and activation in forelimb motor cortex

a, Placement of the grin lens and miniscope above contralateral M1, VNS curf in the neck and its wire connectors on top back of skull. **b,** Left, representative neural ROIs from the field of view of one mouse M1 (n = 156 neurons): neurons are pseudo color labeled as VNS-activated (red) and suppressed (blue), scale bar = 100 µm. Middle and right: two representative neurons' Ca responses aligned by VNS onset (gray: individual trials; red: VNS-activated; blue: VNS-suppressed). **c,** Top: individual neurons' average response z-scored to inactive phases of all neurons from the representative mouse in **b**; bottom: average neural responses of all neurons from the same mouse. **d,** Average % of total neurons activated, suppressed, bidirectionally modulated and nonmodulated after 0.6 to 0.8mA VNS delivery (N = 7 mice, 767 neurons). **e,** % of total neurons that are activated or suppressed by VNS across different current amplitudes. (N = 7 mice, n= 747~807 total neurons from each stimulation group, One-way ANOVA and multiple group comparison to 0~0.1 mA group, * $p < 0.05$, ** $p < 0.01$, *** $p < 0.001$). **f,** Neural response heatmap of all activated neurons and all suppressed neurons aligned at VNS onset. **g,** Average neural activity of all activated neurons and all suppressed neurons aligned at VNS onset (N=7 mice, 82 activated neurons, 125 suppressed neurons, 0.6mA VNS). **h,** Cumulative distribution of neural response peak time of activated and suppressed neurons measured as the peak value of the average trace 0 to 5 seconds after VNS onset (82 to 151 neurons from each group, Kruskal-Wallis test followed by Dunn's multiple comparisons test, $p < 0.0001$).

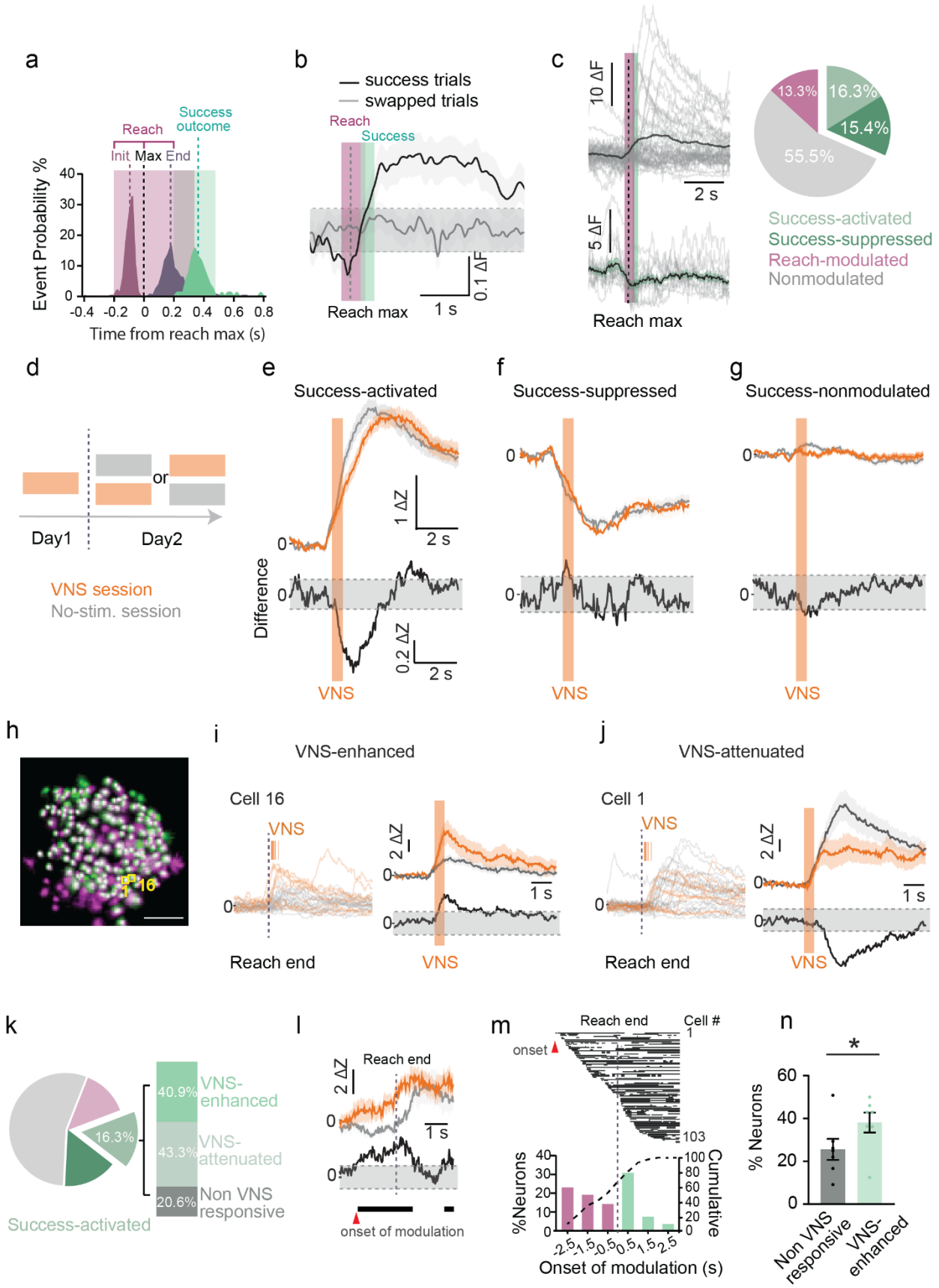
a
Reach
Success outcome
Init Max End
Event Probability %
Time from reach max (s)
b
success trials
swapped trials
Reach
Success
Reach max
1 s
0.1 ΔF
c
10 ΔF
5 ΔF
2 s
Reach max
13.3%
16.3%
15.4%
55.5%
Success-activated
Success-suppressed
Reach-modulated
Nonmodulated
d
or
Day1
Day2
VNS session
No-stim. session
e
Success-activated
1 ΔZ
2 s
Difference
0.2 ΔZ
VNS
f
Success-suppressed
VNS
g
Success-nonmodulated
VNS
h
16
i
VNS-enhanced
Cell 16
VNS
2 ΔZ
1 s
Reach end
VNS
j
VNS-attenuated
Cell 1
VNS
2 ΔZ
1 s
Reach end
VNS
k
40.9%
VNS-enhanced
16.3%
43.3%
VNS-attenuated
20.6%
Non VNS responsive
Success-activated
l
Reach end
2 ΔZ
1 s
onset of modulation
m
Reach end
Cell #
1
onset
103
%Neurons
Cumulative
Onset of modulation (s)
n
*
% Neurons
Non VNS responsive
VNS-enhanced

Figure 7 | Success VNS selectively modulates activities of a subpopulation of task-activated M1 neurons in the reach task.

a, Peri-event histogram of the task related events aligned at reach max (N = 6 control mice, day 4, n = 278 single-reach success trials). Dashed lines indicate median reach initiation -93 ms, reach max 0 s, reach end 180 ms and CLARA success recognition 360 ms. Magenta indicates full reaches, green success recognition. **b**, Average neural activity of success trials (black) and random control trials (grey, n = 488 neurons). Gray dashed line indicates 2 s.d. from the baseline mean. c, Left: representative neural responses: red success-activated, blue success-suppressed, gray individual trials. Right: % neurons modulated in the task (903 neurons; 16.3 ± 6.4% success-activated, 15.4 ± 10.2% success-suppressed, 13.3 ± 5.5% preparation/reach modulated). **d**, Assignment of VNS or no-stimulation sessions. **e-g**, Top: Average responses of success-activated (d,115 and 101 neurons), success-suppressed (e, 122 and 92 neurons) and success-nonmodulated neurons (f, 383 and 394 neurons) in VNS (orange) and in no-stimulation session (gray). Bottom: the difference trace. **h**, Registered neurons (white) in VNS (green) and no-stimulation session (Magenta). **i&j**, Left: trial responses of success-activated neurons in no-stimulation session and in VNS session (orange ticks: trials' VNS onset). Right: the average and difference responses of the same neurons aligned by VNS onset. **k**, Percentage of success-activated neurons (n = 77 registered) that are enhanced (40.9 ± 13.7%) or attenuated (43.3 ± 21.2%) in VNS compared to no-stimulation session. **l**, One success-activated neuron modulated by VNS (supp. Fig. 6h) also have higher neural activity before reach end in VNS session. Arrowhead: onset of increased activity. **m**, Onset timing histogram of VNS-driven modulation of success-activated neurons. n, % neurons modulated in reach in VNS-nonmodulated versus VNS-enhanced neurons.

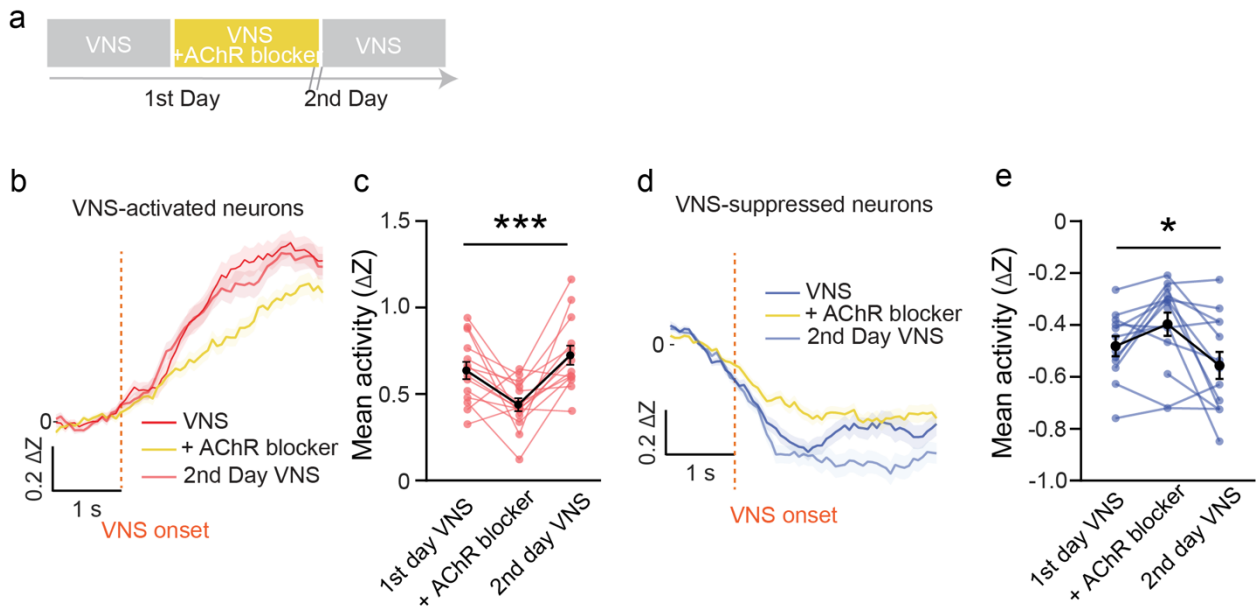

Figure 8 | VNS driven acute neural modulation is mediated through AChRs.

a, Diagram of experimental design: three sessions including a control VNS session in home cage, VNS session with AChR blocker, recovery VNS session on the 2nd day. **b&d,** Average neural activity of VNS-activated neurons (**b,** n = 104 ~116 neurons) or VNS-suppressed neurons (**d,** n = 124~143 neurons) in control VNS session, VNS session with AchR blocker and the 2nd day recovery VNS session. **c,** Average neural activity comparison of VNS-activated neurons quantified from 0.8 to 2.8 seconds after VNS onset, defined based onset and peak delay of VNS-driven neural activation in Figure. 6 (N = 7 mice x two repeats each mouse, Repeated measures ANOVA, $p < 0.001$). **e,** Average neural activities comparison of VNS suppressed-neurons quantified from 0.2 to 1.6 seconds from VNS onset defined based onset and peak delay of VNS-driven neural suppression in Figure. 6 (N = 7 mice x two repeats each mouse, Repeated measures ANOVA, $p = 0.02$,).

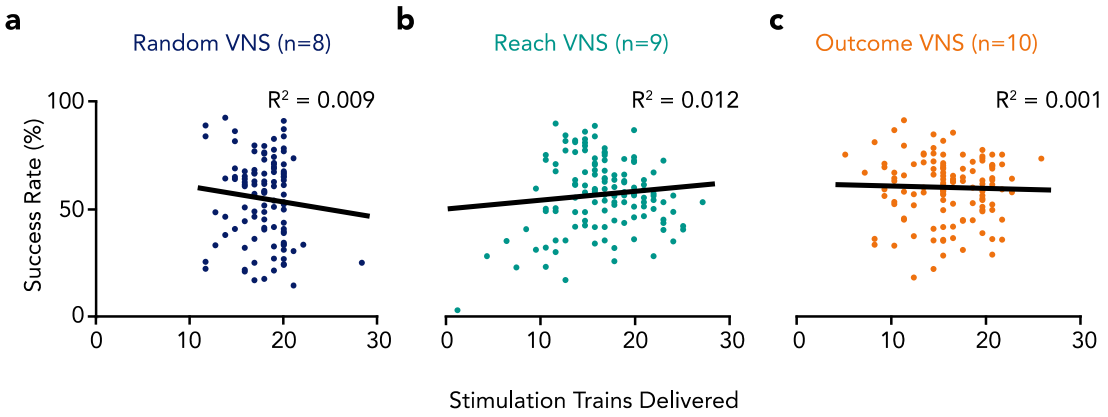

Supplementary Figure 1 | Stimulation Amount between Random VNS, Reach VNS, and Success VNS does not predict success.

a-c, a simple linear regression was calculated to predict success rate based on the amount of stimulation trains given across groups in a particular session. **a,** For Random VNS a regression equation was found (F(1.03) p = 0.3117), with an R^2 of 0.009. **b,** For Reach VNS a regression equation was found (F(2.017) p = 0.22), with an R^2 of 0.011 **c,** For Success VNS a regression equation was found (F(0.11) p = 0.7359.), with an R^2 of 0.001.

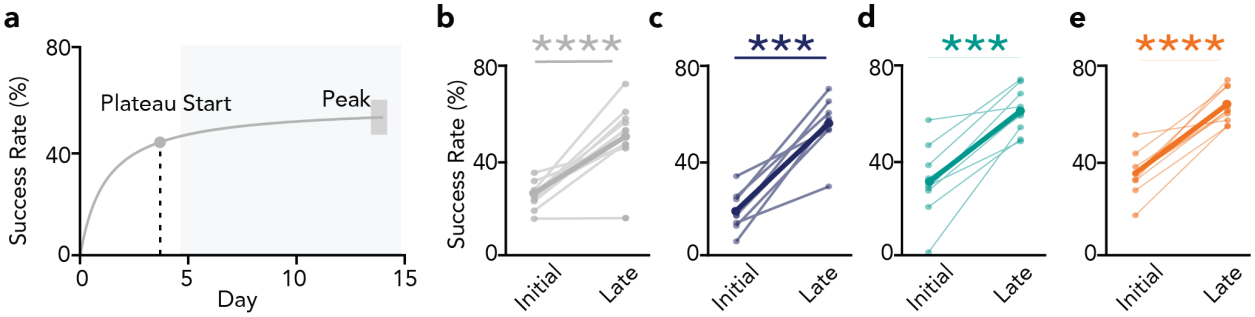

Supplementary Figure 2 | All experiment groups learn the behavior task.

a, nonlinear model of sham animal learning trajectories used to identify early and late learning phases (Methods). **b-e,** Comparison of performance during early and late learning phases in Sham VNS (paired T test, n=12, p=0.0001), Random VNS (paired T test, n=8, p=0.0001), Reach VNS (paired T test, n=9, p=0.0002), and Success VNS (paired T test, n=10, p=0.001).

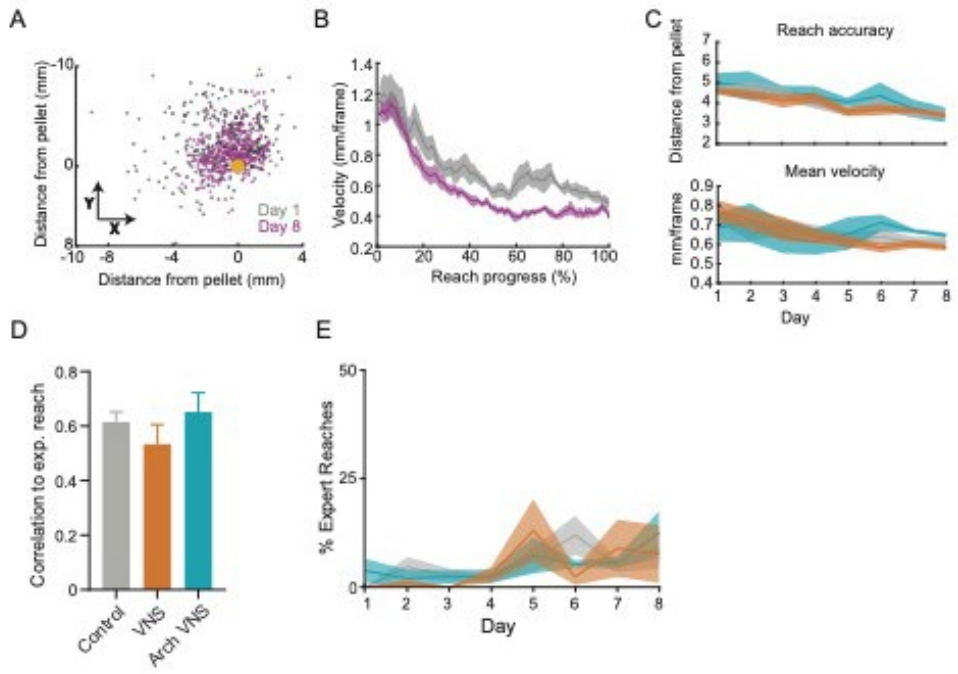

Supplemental Figure 3 | VNS does not change speed, accuracy or initial exploration.

a, Endpoint targeting of all control reaches on day 1 (grey) and day 8 (purple) of learning. Orange dot depicts pellet center. **b**, Mean absolute velocity between reach initiation and reach maximum on day 1 and day 8 of learning. Reaches are time warped to be an equal arbitrary length. **c,** Comparison of endpoint accuracy (top) and absolute velocity (bottom) between control, VNS and Arch+VNS stimulation ($p>0.05$, RM ANOVA, VNS N=8, Arch+VNS N=6, Control N=8). **d,** Reach variability on day 1 for all groups, as measured by average correlation to expert trajectory ($p>0.05$, One-way ANOVA, VNS N=8, Arch+VNS N=6, Control N=8). **e,** Percent of 'Reach Failures' that qualify as expert reaches over learning.

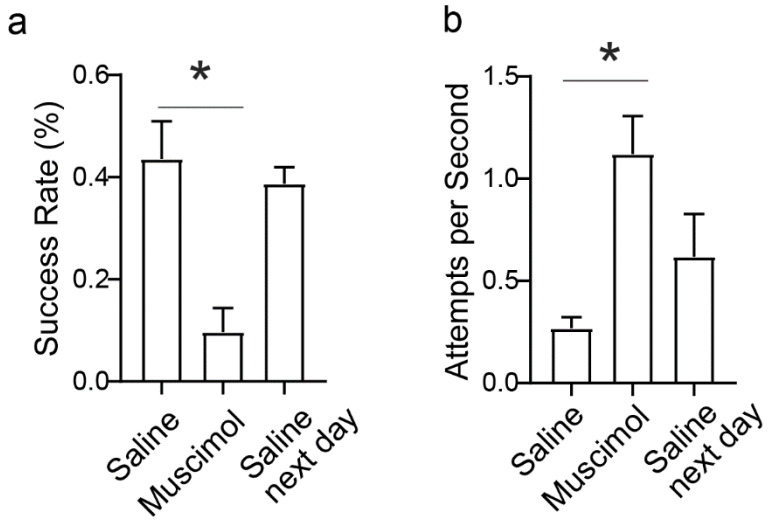

Supplementary Figure 4 | The M1 activity is necessary for successful execution of the skilled reach task.

a, Comparison of success rate of the skilled reach task before and after muscimol infusion into M1 (n = 3 mice, one-way ANOVA, $p<0.05$). **b,** Comparison of reach attempts per second in the same mice before and after muscimol infusion (n = 3 mice, one-way ANOVA, control ~0.3 reaches per minute, muscimol 1.1 reaches, $p<0.05$).

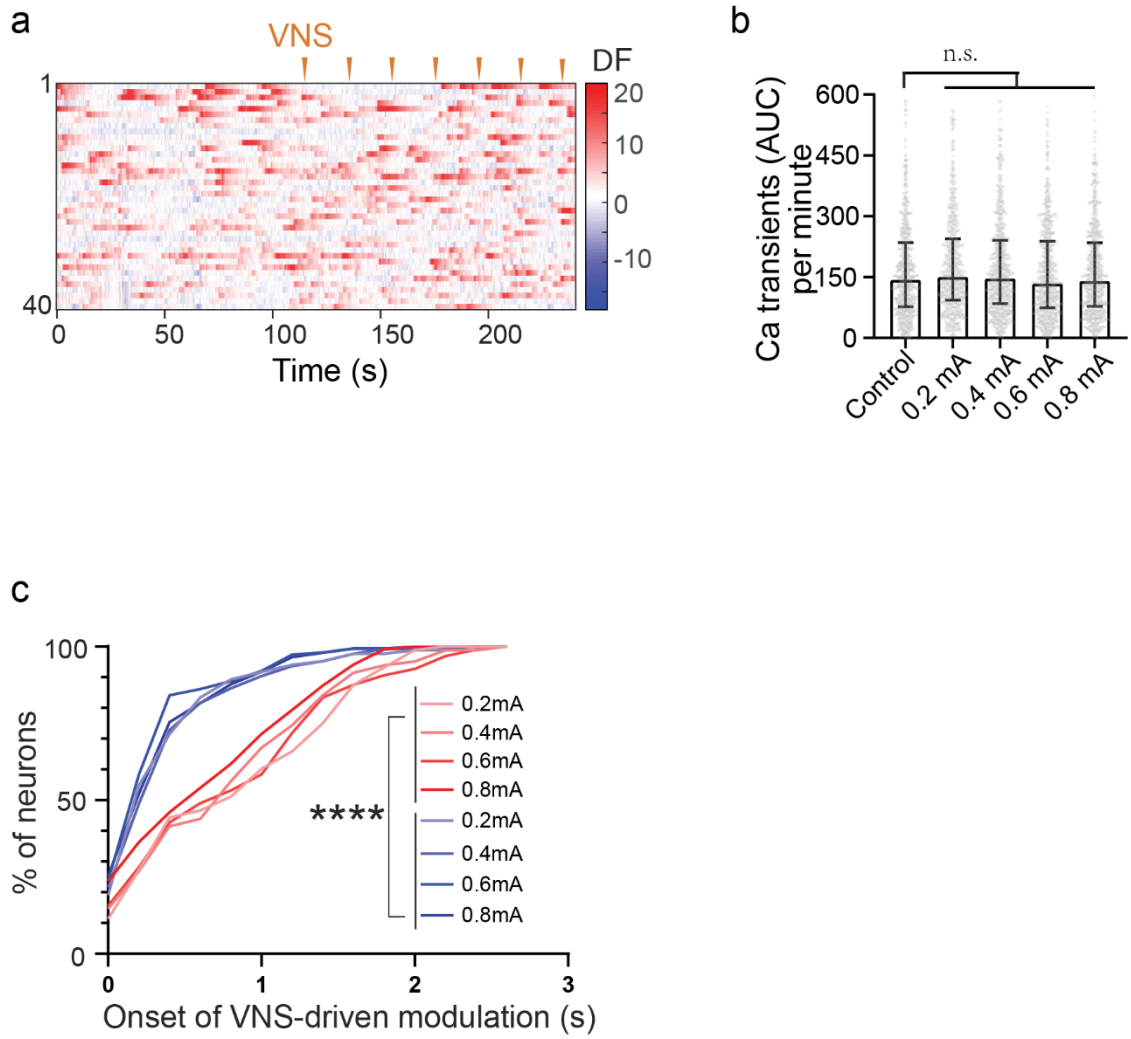

Supplementary Figure 5 | The M1 activity is constant on minutes' time scale and the VNS response onset timing analysis.

a, Heatmap plot of 40 neurons' GCaMP6m calcium response in L2/3 M1 from a representative mouse in homecage two minutes before VNS delivery and two minutes with VNS trains delivery. Each orange arrow indicates one VNS pulse train delivery (15 pulses at 0.1 ms duration, 30 Hz, 0.4 mA). **b,** Ca transients quantified as area under the curve (AUC) of the fluorescence trace per minute in the 2nd minute after VNS application starts in VNS mice (n = 7 mice, 676 to 732 neurons, plot as median with interquantile range. Kruskal -Wallis test followed by Dunn's multiple comparison, $p > 0.05$ for all VNS stimulation groups compared to control. Controls are the same mice without VNS delivery). **c,** Cumulative distribution of neural response onset (measured as the first value goes above 2SD of the baseline mean in the average trace 0~5 seconds after VNS onset) of VNS-activated or suppressed neurons (82 to 151 neurons from each group, 7 mice, Kruskal-Wallis test followed by Dunn's multiple comparisons test, $p < 0.0001$).

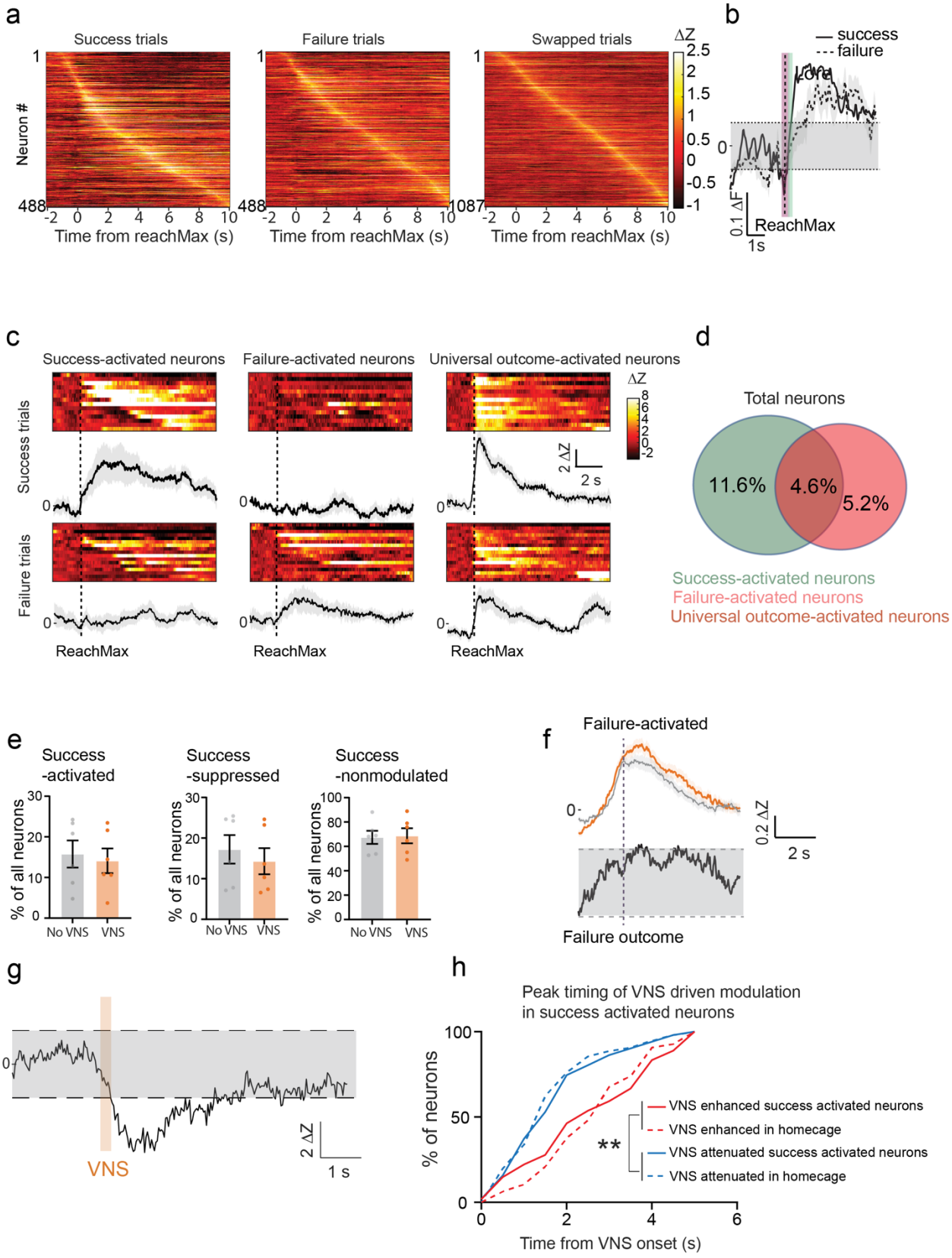
a
Success trials
Failure trials
Swapped trials
Neuron #
Time from reachMax (s)
ΔZ
b
success
failure
ReachMax
1s
0.1 ΔF
c
Success-activated neurons
Failure-activated neurons
Universal outcome-activated neurons
Success trials
Failure trials
ReachMax
2 ΔZ
2 s
d
Total neurons
11.6%
4.6%
5.2%
Success-activated neurons
Failure-activated neurons
Universal outcome-activated neurons
e
Success -activated
Success -suppressed
Success -nonmodulated
% of all neurons
No VNS
VNS
f
Failure-activated
Failure outcome
0.2 ΔZ
2 s
g
VNS
2 ΔZ
1 s
h
Peak timing of VNS driven modulation in success activated neurons
% of neurons
Time from VNS onset (s)
VNS enhanced success activated neurons
VNS enhanced in homecage
VNS attenuated success activated neurons
VNS attenuated in homecage
**

662

Supplementary Figure 6 | The M1 neural dynamics in the reach task.

a, Heatmap plot of individual neurons' response sorted by the peak timing: reach max is 0 second (N = 6 mice, n = 488 neurons). **b,** Average neural activity of all neurons in single-reach success trials (black line), and single-reach failure trials (dotted line). Gray block indicates 2 SD from the baseline mean during -6 to -3 s before reach max. **c,** Heatmap plot of trials and average response of representative success-activated neuron, failure-activated neuron and universal outome-activated neuron aligned by reach max. **d,** % of success activated-neurons, failure-activated neurons and universal outome-activated neurons (1 mice, 172 neurons). **e,** The percentage of success-activated, -suppressed and non-modulated neurons in VNS sessions and in no-stimulation sessions (N = 6 mice, total 488 neurons). **f,** Average neural activity of failure-activated neurons in VNS session (orange, 77 neurons) and in no-stimulation session (gray, 73 neurons), aligned at outcome recognition by CLARA. **g,** Cumulative distribution of neural response peak time of VNS enhancement or attenuation of outcome-activated neurons' outcome response. The VNS driven enhancement or attenuation are measured as the peak value of the difference trace (individual neuron's VNS session average – no-stimulation session average) 0~5 seconds after VNS onset (51~54 neurons from each group, 6 mice, Kruskal-Wallis test, $p < 0.0001$). **h,** The response to VNS of representative success-activated neuron in fig. 7l aligned at VNS and normalized to the -3 ~0 seconds before VNS.

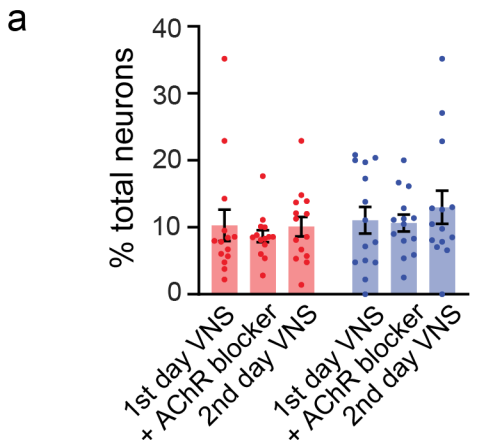

682

683 **Supplementary Figure 7 | The neural populations analysis with AChR blocker.**

684 **a,** Percentage of VNS-activated neurons and VNS-suppressed neurons in the total neuron populations after

685 0.4~0.6 mA VNS delivery in control VNS session, VNS session with AChR blocker, recovery VNS session

686 2nd day (N = 7 mice. total 627 neurons, Brown-Forsythe ANOVA test, $p > 0.5$)

687

688

689

690

691

692

Methods

Animal care

All animal procedures and experiments were performed in accordance with protocols approved by the Institutional Animal Care and Use Committee at the University of Colorado Anschutz Medical Campus. Male and female adult C57BL/6 wild-type mice between the age of 2 and 10 months old were used for all experiments unless otherwise noted. Mice were group-housed before surgery and single-housed following surgery and throughout behavior training. Mice were kept on 14h light/10h dark schedule with ad libitum access to food and water with exception from behavior-related food restriction (Forelimb Reach training).

Surgery

Vagus nerve stimulating cuff implantations

Commercial cuffs from Micro-leads (150um cuffs) and Cortec (100 um microsling cuffs) soldered to gold pins or Plastics1 connectors were implanted on the cervical vagus nerve. Mice were anesthetized with 4.5% isoflurane anesthesia for induction and maintained with 1.5%. 1% injectable lidocaine was used locally at incision sites. Eye ointment was applied to the eye to prevent corneal drying. Temperature was regulated at 37ºC with a thermostat-controlled heating pad. The vagus nerve was accessed with an incision in the ventral cervical region, and the nerve was bluntly dissected from the carotid sheath. The cuff was tunneled subcutaneously to the ventral cervical incision from an incision at the base of the dorsal skull. The vagus nerve was placed in the cuff. Kwik-Sil (WPI)The ventral cervical incision was sutured using 6-0 absorbable sutures. The dorsal skull was cleaned using saline and ethanol, and electrical connectors were fixed to the skull using dental cement (C&B Metabond). GLUture (WPI) was used to seal the skin around the dental cemented headcap. Stimulation efficacy was measured using peripheral biomarkers such as breathing rate changes and heart rate reduction[25] on the day of surgery and weekly until the end of experiments with paw sensor (Mouse Stat Jr., Kent Scientific). Mice received sub-cutaneous lactated ringers (~100µL as necessary), intramuscular gentamicin (3mg/kg), and intraperitoneal meloxicam (5mg/kg) following surgery and as needed in cases of dehydration, infection, or pain. Mice were monitored for 7-14 days to ensure proper recovery from surgery before any subsequent experiments were conducted.

Viral injections and optical fiber implantation

All surgeries were performed on mice that express Cre recombinase driven by the ChAT promoter (ChAT-IRES-Cre, Jackson Labs stock #0064100 [97]). Animals were prepared for surgery as described above, and the hair was removed prior to an incision over the dorsal skull. 200um diameter fiber optics with 1cm ceramic cannulas were fabricated in-house using ONECore facilities. The skull at the dorsal incision was cleaned using sterile saline and ethanol. Two craniotomies were opened above the basal forebrain in each

727 hemisphere (0.35mm posterior, ±1.6mm lateral of bregma) using a dental drill. Glass pipettes containing a
728 floxed inhibitory archaerhodopsin (AAV-EF1a-DIO-eArch3.0-EYFP, UNC) or YFP control (AAV-EF1a-
729 DIO-EYFP-WPRE-pA, UNC) were then inserted bilaterally into the basal forebrain using a stereotaxic
730 device (-4.75mm from dorsal surface of the brain). Approx. 210nL of viral construct was injected over 5
731 minutes. The pipettes were removed and 200um fiber optic cannulas were inserted above each injection site
732 (-4.65mm from the dorsal surface of the brain). The craniotomies were then sealed using a surgical silicone
733 (Kwik-Sil). The cannulas were fixed to the skull using dental cement (C&B Metabond). Gluture was used
734 to seal the skin around the headcap. Mice received intramuscular gentamicin (3mg/kg), and intraperitoneal
735 meloxicam (5mg/kg) following surgery and as needed in cases of infection, or pain. Mice were monitored
736 for 5-7 days to ensure proper recovery. After 14 days, mice underwent VNS implantation described above
737 (see Vagus nerve stimulating cuff implantations).
738
739 *Electrode implantation*
740 Chronic tetrodes: Custom twisted wire tetrodes, built in-house, were implanted into the left basal forebrain
741 of mice. Surgical preparation was as described above. Then, two craniotomies were opened using a dental
742 drill; one above the left basal forebrain (0.35mm posterior, 1.6mm lateral of bregma) and one above the
743 cerebellum (~1mm posterior of lambda, midline). A tetrode was then inserted into the basal forebrain
744 craniotomy using a stereotaxic device (-4.75mm from the dorsal surface of the brain). A gold ground pin
745 was inserted into the cerebellum. Both craniotomies were sealed with surgical silicone (Kwik-Sil) and the
746 tetrode was fixed to the skull using dental cement C&B Metabond). Gluture was used to seal the skin around
747 the dental cemented headcap. Mice received intramuscular gentamicin (3mg/kg), and intraperitoneal
748 meloxicam (5mg/kg) following surgery and as needed in cases of infection, or pain. Mice were monitored
749 for 7 days to ensure proper recovery after which they underwent VNS implantation described above (see
750 *Vagus nerve stimulating cuff implantations*).
751
752 Acute Optrodes: Vagus nerve cuffs were implanted in transgenic mice expressing Channelrhodopsin2 in
753 cholinergic neurons (ChAT-ChR2 [98]) using the protocol described above (see *Vagus nerve stimulating cuff*
754 *implantations*). After cuff implantation, while mice were still under anesthesia (1.5% isoflurane), mice were
755 moved to a stereotaxic apparatus and a cranial window (2.5x2.5mm) was opened above the left BF (0.35mm
756 posterior, 1.6mm lateral of bregma). The stereotaxic apparatus was placed in a Faraday cage and single
757 shank Optrodes from Neuronexus (A1x32-Edge-10mm-20-177-OA32LP) were inserted into the BF (-
758 4.75mm from the dorsal surface of the brain). Extracellular recordings were then performed while mice
759 then underwent VNS (see *BF response to VNS*) and Opto-tagging (see *Opto-tagging*) protocols. Mice were
760 sacrificed at the end of the experiment and the cuff and optrode were recovered.

761

762 *Cranial window surgery for miniscope objective lens and baseplate installation*

763 Mice were anesthetized with isoflurane and maintained similarly as described above until skull is exposed.
764 A round cranial window (~1.8mm diameter, ML 1.5mm, AP 0.3 mm for center) was made on contralateral
765 M1 using a dental drill. A viral vector (AAV1.Syn.GCaMP6m.WPRE.SV40) was infused at $2x10^{12}$ titer
766 to 200 ~300 um beneath brain surface at 3~4 sites in the cranial window around the center, with ~200 nl
767 each site. Objective grin lenses (Edmund Optics, #64520, 1.8mm, 0.23mm WD) were lowered through the
768 cranial window and pressed against the brain surface. The lens' side was sealed by surgical silicone (Kwik-
769 Sil) and secured by dental cement. The exposed part of the lens above the skull was further coated with
770 black nail polish. 3~4 weeks later, a metal baseplate was mounted to the skull over the lens with loctite glue
771 (loctite 454 prism), guided by miniscope for optimal field of view while the mouse were anesthetized with
772 isoflurane (1.5%). After the baseplate were securely mounted, the miniscope was taken off, a cap was
773 attached to the baseplate and the mouse was returned to homecage.

774

775 *Muscimol cannula surgery and infusion*

776 With the same craniotomy surgery procedure described above, a round cranial window (~1.8 mm diameter,
777 ML 1.5mm, AP 0.3 mm for center) was made on contralateral M1 and a plastic cannula (2~3 mm long pipet
778 tip) was inserted into the window right above the brain surface. Then the pipet tip was secured by kwik-sil
779 and dental cement. The top of the cannula will be sealed with kwik-sil if the mouse is not going to the
780 behavior test in a couple of hours. Before behavior tests, the mice were briefly anesthetized with isofluorane
781 the seal will be removed and 1~2 μL of muscimol at a concentration of 1 mg/mL will be infused into the
782 pipet tip.

783

784 **Behavior**

785 *Manual training of skilled forelimb reach task*

786 Mice were trained and scored on a skilled reach task [99]. Mice were food restricted and maintained at 85-
787 90% of their weight throughout training. Following food restriction, mice were habituated to the training
788 box for 20 minutes where mice were given 20mg food pellets (BIO-serv) near the window of the box where
789 reaching occurs. The training box is a custom-built plexiglass box with a 1cm wide opening that provides
790 access to a platform or post with a divot to hold a pellet located approximately 1cm away with a left offset
791 from the center of the opening to force right forepaw reaching. Learning sessions then occurred for 14
792 consecutive days where mice perform a reach to grasp task with the right forepaw for food pellets. Rehearsal
793 sessions occurred 7-10 days after training and featured stimulated and unstimulated trials. For both training
794 and rehearsal sessions, mice were scored on a per trial basis until 20 successful attempts or 20 minutes

passed. A trial terminates in a success or the pellet being knocked off the pellet holder by the mouse. Trial outcomes were recorded by the trainer in real time. A success was defined by when the mouse grabbed the pellet and returned it into the cage. Errors were subcategorized into: “reach error” (failure to correctly target), “grasp error” (failure to grasp the pellet), and “retrieval error” (successful grasp of pellet, but failure to return it into the box).

VNS experiment groups

Experiment groups for training were based on stimulation protocols. Sham VNS cohort were implanted with a cuff but were not stimulated at any point during learning. Success VNS were manually stimulated following every successful trial -- days 7 and 14 featured designated blocks without stimulation to track baseline learning levels versus trial-to-trial performance. Reach VNS received manual stimulation prior to movement onset on a pseudo-random 50% subset of trials to normalize VNS trains delivered. Random VNS received stimulation at random intervals as generated by an Arduino board to achieve between 15-20 stimulations per day, matching stimulation rates to other groups. All groups were trained on the forelimb reach task for 14 days, Reach VNS and Success VNS were tested during rehearsal in naively trained mice.

CLARA training and behavior data acquisition

Mice were food restricted and habituated identically to manually trained animals. Dimensions of the behavior box were also identical in manual and CLARA cohorts. Behavior box used for miniscope recording was modified so that the front panel had an alcove above the height of mouse head to accommodate the miniscope when the mouse was close to the slit to reach. On day 1, the mice were primed to have one success before CLARA training session started. Learning sessions then occurred for 14 consecutive days (or specified otherwise in results) where mice perform a reach to grasp task with the right forepaw for food pellets. Each trial started as the automated dispenser placing a food pellet on the post, as the mouse reached to successfully retrieve it or knocked it off, the CLARA would mark success or failure as the trial outcome as the end of this trial. Each session lasted for 20 minutes and mice were scored on a per attempt basis. Using the CLARA behavior system, high speed (150hz) video data was recorded from three FLIR Blackfly® S (model BFS-U3-16S2M-CS, Edmund Optics) cameras placed in front of the box, lateral to the box, and at 45° angle above the box from the opposite side from the lateral camera (**Fig. 6a**). A neural network was trained prior to experiment sessions using manually annotated frames of the skilled reach behavior labeling the hand center and the pellet. Video frames from all cameras we sent through this network in real time to identify the location and state of the hand and pellet. This information was used initiate trials via pellet placement and to categorize attempt outcomes as either success or failure so that stimulation could be delivered in a closed-loop manner (for additional details, see [40]). The timing of pellet

829 placement, success or failure outcome, VNS delivery, and optogenetic light delivery were recorded through
830 CLARA. In miniscope cohort, the timing of miniscope neural recording is cross registered with behavior
831 video frames through CLARA controlled arduino board.
832
833 *Optogenetic+VNS experiment groups*
834 Experiment groups for training were based on stimulation type. The control cohort was injected with a
835 floxed YFP construct that did not contain an opsin and received light stimulation (see *Light stimulation*
836 *parameters*), the Success VNS cohort was electrically stimulated (see *VNS stimulation parameters*), and
837 the Arch w VNS cohort received both light and electrical stimulation. All groups automatically received
838 stimulation following every successful trial through the CLARA system.
839
840 *Miniscope groups*
841 Mice wore miniscopes for 5~10 minutes for a few times in their home cages or CLARA training box to
842 habituate the weight. When recording VNS response in homecage, mice wearing miniscopes and VNS
843 wires were put in homecage. About 4 minutes spontaneous neural activity were recorded as mice freely
844 moving in homecage, then 30~40 VNS were delivered every 20~30 seconds. Afterward, another ~4
845 minutes spontaneous activity were recorded. In sessions with AChR antagonists, scopolamine (1 mg/kg
846 body weight) and mecamylamine (10 mg/kg body weight) were dissolved in saline and delivered to mice
847 through Intraperitoneal (IP) injection. The concentration of scopolamine and mecamylamine cocktail was
848 chosen to have effects in brain circuits of memory and learning without debilitating effects according to
849 previous studies [100,101]. After 15 minutes, the neural response was recorded in homecage session.
850 For reach training recording, food restricted mice were mounted with miniscope and VNS wires and put in
851 training box to start CLARA training session. The minisope acquisition was turned on immediately as
852 CLARA training session started and each frame of the video was cross registered with the CLARA video
853 frames. All mice were primed without VNS to have one success reach before the first session started. On
854 the first day, VNS mice participated in one 20 minutes' Success VNS session. From day 2 to day 4, each
855 VNS mouse participated in two sessions of training, with one of them being a Success VNS session, the
856 other a no-stimulation session in which VNS was not delivered, given on a pseudorandomized schedule
857 (Fig. 7d). Control mice also received two training sessions without VNS each day. On days when mice
858 receive two sessions of training, the two sessions are 1~3 hours apart.
859
860 *Place preference test*
861 We used a standard conditioned place preference test to examine if VNS is rewarding or aversive. The
862 behavior apparatus contained two compartments separated by a gate. Mice were tested for baseline

preference in an initial 20-minute session where mice can freely navigate between compartments. Mice then were trained for three days with two 20 minute sessions each day where they received stimulation in only one compartment. Stimulation was delivered pseudo-random approximately once per minute. On the day of testing, no stimulation was given, and mice were tested to see which compartment they spent more time in [102]. The amount of time spent in each compartment was compared between the baseline and testing day. Experiments conducted with assistance from CU Anschutz Behavior Core.

Stimulation parameters

<u>VNS stimulation parameters</u>

For all VNS experiment groups, VNS was delivered as a 500ms train of 15 pulses with 100µs phase duration at 30Hz. Current amplitudes were 0.4-0.6mA. Stimulation parameters were controlled and delivered using Master8, PulsePal, or CLARA+Arduino connected to a stimulation isolation unit (A-M Systems, Model 2200 Analog Stimulus Isolator) to control amperage.

<u>Light inhibition parameters</u>

For all light stimulated groups, 561nm light was delivered continuously for 500ms. Light was delivered through a 200nm fiber-optic cable from a Class IIIb diode pumped solid state laser (Cobalt) at 0.5mW (calculated based on output efficiency from the bottom of the optical fiber).

Behavior and kinematic analysis

Manual behavior analysis

A success percent was generated for each session of each animal by determining the number of trials that resulted in a successful retrieval out of all trials initiated. Success percent was compared between stimulation groups across all days of training, as well as by early and late learning phases. Early learning phase refers to days 1-4 of training, Late phase refers to days 5-14 and were defined using a Weibull growth curve (See Quantification and Statistical Analysis). On days where animals received blocks of stimulation, such as rehearsal groups, stimulated and unstimulated trials were compared on a per mouse basis within days.

Behavior curator analysis

Videos acquired during CLARA training sessions were processed by custom python scripts overnight to extract key reach timepoints: reach initiation (ReachInit), when the hand leaves the box; reach max (ReachMax), the outward point of maximum distance from reach initiation; reach end (ReachEnd), when the hand returns to the cage; and stimulation onset (stim), when a trial received a trigger pulse for VNS or

897 light stimulation. The stamps of reachInit, reachMax and reachEnd were further manually screened for
898 consistency. The accuracy of CLARA trial outcome classifications were verified, and failures were
899 subcategorized *post-hoc* into reach, grasp and retrieval failures.
900
901 *Kinematic analysis*
902 3D Tracked data of paw center and pellet were tracked during reach attempts (between reach initiation and
903 reach end) were extracted using custom MATLABMATLAB scripts (MATLAB Simulink) and
904 documented as 3D data arrays for kinematic analysis. and documented as 3D data arrays.
905 Positional data for gross targeting experiments was determined by selecting the 3D location of the hand and
906 pellet at the reach max timepoint. Points were normalized such that the pellet center was 0,0,0. Euclidean
907 distance between the hand center and pellet center was then calculated using the norm function from
908 MATLAB. The mean distance from pellet was compared in early and late phases and between stimulation
909 groups. Reach velocity was obtained by measuring the absolute velocity between reach initiation and reach
910 end and averaging the velocity over that period. The mean velocity was compared in early and late phases
911 of training and between stimulation groups.
912
913 *Reach consistency and expert reach*
914 Positional data between these timepoints were then normalized such that the pellet center was 0,0,0. Reach
915 trajectory was defined as the time between reach initiation and reach end. Each trajectory was then
916 temporally warped to be the same arbitrary 'length' of time using dynamic time warping[103]. An expert
917 expert trajectory was constructed for each mouse by averaging the trajectories of all successful reach
918 attempts made on each mouse's last two days of training. Reach consistency was determined through
919 comparison of reach trajectories to each mouse's expert trajectory. Reach trajectories were compared to the
920 expert trajectory through a correlation coefficient to obtain the mean correlation coefficient for each mouse
921 in each training session. Additionally, any individual reach that had a correlation of 0.95 or higher with the
922 expert trajectory was defined as an 'expert reach', and the percent of expert reaches were also recorded for
923 each day. Number of expert reaches and mean correlation coefficients were then compared between VNS,
924 Arch+VNS and control groups in early and late phases.
925
926 *Feature consistency*
927 Several reach features were extracted from each reach attempt: Start location (X, Y, Z), End location (X,
928 Y, Z), Mean absolute velocity, Max absolute velocity, Pathlength (length of full trajectory, and Reach
929 consistency (defined above). The distribution of each feature was calculated for the early and late learning
930 phases based on the stimulation group. The distribution of each early-late pair was normalized using the

interquartile range of the early phase distribution. The normalized late interquartile range was subtracted from the normalized early range and the difference was defined as 'delta feature consistency'. A positive delta means that the distribution was tighter during the late phase compared to the early phase.

Electrophysiology recording and analysis

VNS electrophysiological recording in BF

While mice were either under maintained anesthesia (1.5% isoflurane), or awake in a homecage, VNS was repeatedly delivered while recording from the left basal forebrain (see Optrode implantation). No behavioral task was performed during recording. Mice received several (10-20) trains of VNS (0.5s, 30hz, 100us pulse-width, 0.6mA), delivered approximately 90 seconds apart. Data was recorded with Cheetah acquisition software at 30kHz using a Digital Lynx SX (Neuralynx). TTL pulses were sent from the Master-8 (A.M.P.I.) to the Digital Lynx SX for each pulse of a light or electric stimulation train. In acute experiments, mice were opto-tagged after all VNS trains were delivered to identify cholinergic units.

Opto-tagging protocol

While mice were under maintained anesthesia (1.5% isoflurane), recordings were performed in the left basal forebrain (see Optrode implantation). Light was delivered using a class 3b diode pumped solid state laser (Cobalt) attached to the optrode through a ceramic ferule. Opto-tagging stimulus consisted of several (10-20) trains of 5mW 488nm light delivered just above the basal forebrain through a 105um diameter fiber optic spaced ~30 seconds apart. Trains consisted of 10 pulses of light at 20hz with a 10ms pulse duration.

Neural classification of BF response

After recording, units were clustered manually using clustering software SpikeSort 3d (Neuralynx) and imported into MATLAB. Isolation distance and L-ratio were used to quantify cluster quality and noise contamination[104]. The start of each train was identified post hoc using custom scripts (Mathworks) and defined as a trial. The trial window, referred to as the 'VNS stimulation window' was defined as a 1 second baseline before stimulation (-1 to 0s), VNS delivery (0 to 0.5s) and 1 second after the end of VNS (0.5 to 1.5s). Firing rate during the trial window was calculated using a 100ms moving average, shifted by 1ms from the start of the trial window to 100ms after the end of the trial window. Baseline firing rate was defined as the mean firing rate during the baseline period (-1 to 0s). Units were screened, and any unit with a mean firing rate below 0.5Hz in anesthetized recordings or below 1Hz in awake recordings were removed from the pool. +/-1ms around each stimulation pulse was removed to account for electrical noise. Firing rate was converted into a Z score normalized to the mean firing rate and standard deviation baseline activity. If a unit's normalized firing rate was ±2.56 s.d. from baseline firing rate for >100ms during the VNS delivery

965 window (0 to 0.5s), the unit was defined as VNS responsive. If the change in firing rate was 2.56 s.d above
966 baseline it was further subclassified as Activated, and if it was 2.56 s.d. below baseline, it was subclassified
967 as Suppressed. A unit that met both criteria was classified based on which occurred first. Peak response,
968 peak delay and response duration were compared between cholinergic and non cholinergic units in
969 anesthetized mice, and units recorded in awake mice. Peak response refers to the maximum normalized
970 firing rate of VNS activated units after stimulation onset (0 to 1.5s). Peak response delay refers to the
971 amount of time in ms from train onset (0s) to peak response. Duration refers to the total amount of time that
972 a VNS activated unit had normalized activity <2.56 s.d above baseline after stimulation onset (0 to 1.5s).
973
974 *Neural classification of opto-tagging in BF*
975 After recording, units were clustered manually using clustering software SpikeSort 3d (Neuralynx). Each
976 pulse was identified post hoc using custom MATLAB scripts (Mathworks) and defined as a trial. Tagged
977 units were identified using a stimulus-associated latency test (SALT,[18]). This test compares the distribution
978 of onset time of the first spike recorded during light delivery trials (10ms) to the onset time of spikes during
979 control windows of similar length (10ms). Units whose p-value from the SALT test was <0.05 were defined
980 as cholinergic, all other units were defined as non-cholinergic. Firing rates of cholinergic and non-
981 cholinergic units were calculated using the baseline firing rate of the unit from the VNS session.
982
983 **Calcium imaging and analysis**
984 *Data aqcuisition*
985 Miniscopes components an DAQ board were purchased and assembled by Optogenetics and Neural
986 Engineering (ONE) core according to UCLA miniscope (http://miniscope.org/) V3 guidelines. The
987 objective GRIN lens were Edmund optics # 64-520 and achromatic lens were #45-407. Images were
988 acquired at 30 Hz with MiniscopeControl data acquisition package. affiliated with UCLA miniscope. Each
989 imaging session was 15~20 minutes homecage or CLARA reach training session. The calcium signal
990 images were saved as TIFF stacks through USB3.0 port to SSD hard drive to reduce frame drops. For some
991 homecage sessions, the mice behavior was recorded simultaneously by a LG webcam controlled by
992 MiniscopeControl. For CLARA reach training session, behaviors were recorded by the CLARA system
993 and the timing of miniscope frames and behavior camera frames were coordinated.
994
995 *Imaging analysis*
996 *Neural signal preprocessing*
997 Image stacks acquired through miniscope were motion corrected using NoRMCorre packages
998 [105](https://github.com/flatironinstitute/NoRMCorre). For most sessions, rigid motion correction module

was sufficient to yield good results; in sessions with non-even shifting of the field of view, non-rigid motion correction module was used. After motion correction, the field of view was cropped and spatially down sampled 4x to reduce the file size for subsequent neural signal extraction. The neural signal were extracted from images with CNMF-E package [106](https://github.com/zhoupc/CNMF_E). The results were manually curated to discard non-neuronal ROIs. The result C-raw matrix which was a scaled dF x ROIs was used for further analysis. For individual ROI, the time series dF of the whole session was further organized as 2D matrix dF per trial x trials.

Neural classification

To identify VNS responsive neurons, each trial's dF were organized 10 seconds before VNS onset and 10 seconds after, z-scale normalized to the dF values 3 seconds prior to the onset of VNS for each trial. We call this trial-based z-score process which normalizes baseline period's average to 0 and disregards spontaneous activity's effects on baseline dF level. Average z-scored dF of individual neurons was the average of all trials of dF of the neuron. The response of individual neurons to VNS was measure as maximum and minimum value of the average z-scored dF in the 3 seconds after VNS onset. Noise response was estimated by calculating average z-scored dF for individual neurons using randomize VNS onset time in the same session (excluding the 3 seconds window after each VNS onset in the whole session) and by pooling 1000 repeats of such randomized procedures. For individual neuron, if the real maximum z-scored dF in the 3 seconds window after VNS is higher than 95% value of the 1000 randomized maximum z-scored dF for that neuron, the neuron was defined as activated by VNS; if the real minimum z-scored dF in the 3 seconds window after VNS is lower than 95% value of randomized z-scored dF, the neuron was defined as suppressed by VNS. The bi-directional modulated neurons were rare.

To measure the onset or peak timing for the VNS response, VNS responsive neurons' dF were z-scaled with the whole session baseline mean calculated from time points lacking Ca2+ activity [107](defined as time points with fluorescence values less than the 0.50 quantile of all fluorescence values). This general-based z-score process allows dF level above or below 0 before VNS onset each trial and keeps the average dynamics of VNS response better. For individual VNS activated neurons, the onset of VNS activation was the first time point when the z-scored dF value in the 5 seconds after VNS onset reached above 2 s.d. of the mean of 3 seconds baseline before VNS onset. For individual VNS suppressed neurons, the onset of VNS suppression was the first time point when the z-scored dF value in the 5 seconds after VNS onset reached below 2 s.d. of the mean of 3 seconds baseline before VNS onset.

To identify reach task responsive neurons, similar trial-based z-score process where employed. Trial dFs were aligned by reach max. The baseline was taken as -6 to -3 seconds before reach max time. The response of individual neurons to the task was measure as maximum and minimun value of the average z-scored dF

in the -800 to -300 ms (reach preparation), -300 to 200 ms (reach), 200 to 1700 ms (outcome) in reference to reach max as time 0. The cut off value for maximum or minimum dF for these time windows were estimated by similar randomization procedure as above in which that the same number of reach trials were randomized across the whole session 1000 times. Success trials and failure trials were analyzed separately unless noted otherwise. Several sub-groups of neurons were categorized as preparation-activated, preparation-suppressed, reach-activated, reach-suppressed, success-activated, success-suppressed, failure-activated and failure- suppressed. Preparation and reach modulated neurons were grouped together as reach modulated neurons in figure 7. After neural classification, general-based z-score procedure were used to obtain average success modulated neurons response VNS and no-stimulation sessions.

Cross-registration of multiple sessions and cross session VNS modulated neurons definition

Due to computation power limit, we chose to process neural activity data from each session and register neurons across sessions. CellReg package was used [108] https://github.com/zivlab/CellReg) to identify the same neurons from multiple sessions based on spatial footprints of cellular activity (ROIs). Pairs of neurons with correlation > 0.65 were regarded as the same neurons.

For individual neurons, if it was categorized as success-activated neurons in one of the two training sessions, the neuron is regarded as a success-activated neuron. To look for significant modulation after VNS onset in VNS sessions of these success activated neurons, the success outcome response of individual neuron was aligned to VNS onset and measured in no-stimulation session and VNS session; the difference response was obtained by no-stimulation response - VNS session response. The difference response in the 0~3s after VNS onset that was higher or lower than 2.5 standard deviation of the mean of baseline (-3 to 0 before VNS onset) for at least 0.15 s was regarded significant enhancement or attenuation in the VNS session. To look for significant modulation before VNS onset, the neural response was aligned to reach end. The baseline window was set from -6 to -3 seconds before reach end. This Reach end alignment allows us to evaluate differences in neural representation of reach preparation, execution, and outcome. Differences between the reach representation were compared between the Success VNS and no-stimulation sessions. The difference response in the -3 to 3s around reach end that was higher or lower than 2.5 standard deviation of the mean of baseline (-6 to -3 in reference to reach end) for at least 0.15 s was regarded significant enhancement or attenuation. The onset time of the modulation was defined as the first time point of this enhancement or attenuation.

The control sessions, AchR antagonists and recovery sessions were processed similarly as VNS stimulation in homecage sessions described above. In addition, these sessions were temporally downsample to 15Hz frame rate to reduce file size so that each mouse's three sessions imaging data were motion corrected and concatenated together to save the post hoc cross registration step. For VNS-modulated neurons, the VNS

activation window was empirically measured and defined as rise onset to peak timing in **Fig. 6g&h** (0.8 to 2.8 seconds after VNS onset, suppression window as 0.2 to 1.6 seconds after VNS onset).

Quantitation and Statistical Analysis

Statistical analyses were conducted using Graphpad, JMP (SAS), or MATLAB (MathWorks). No normality tests were performed but individual data points are plotted to visualize distribution. We used parametric statistics including paired and unpaired Student's t-tests, or one-way ANOVA with Tukey's HSD post-hoc tests. Two-tailed tests and $a < 0.05$ were employed unless otherwise stated. We employed a mixed model (Restricted Maximum Likelihood model (REML)) for all learning experiments. REML enables us to test how fixed effects (dependent variables) and known random effects (individual mouse, sex, age) correlate to an outcome variable.

$$\textit{Outcome} = \textit{fixed effect} + \textit{known random effect} + \textit{error}$$

Models were constructed with one or two fixed effects. In cases where there were two fixed effects, we ran full factorial models.

To determine early and late phases of learning a Weibull growth curve was applied to Sham VNS learning data. The formula: $a*(1-\mathrm{Exp}(-(\mathrm{Day}/b)^c))$ a = asymptote, b = inflection point, c = growth rate. The AICc = 1295.90 and the $R^2 = 0.21$. We used the asymptote (55.50% +/- 6.8%) to represent the plateau in success rate. The late learning phase was selected based on which training day exceeded the lower 95th percentile of the asymptote (42.15%) which was day 4. We thus called late learning days 5-14 and early learning days 1-4.

1093 1. Ben-Menachem, E. *et al.* Vagus Nerve Stimulation for Treatment of Partial Seizures: 1. A
1094 Controlled Study of Effect on Seizures. *Epilepsia* **35**, 616–626 (1994).
1095 2. The Vagus Nerve Stimulation Study Group. A randomized controlled trial of chronic vagus
1096 nerve stimulation for treatment of medically intractable seizures. The Vagus Nerve
1097 Stimulation Study Group. *Neurology* **45**, 224–230 (1995).
1098 3. Rush, A. J. *et al.* Vagus Nerve Stimulation for Treatment-Resistant Depression: A
1099 Randomized, Controlled Acute Phase Trial. *Biological Psychiatry* **58**, 347–354 (2005).
1100 4. Shi, C., Flanagan, S. R. & Samadani, U. Vagus Nerve Stimulation to Augment Recovery
1101 from Severe Traumatic Brain Injury Impeding Consciousness: A Prospective Pilot Clinical
1102 Trial. *Neurol Res* **35**, 263–276 (2013).
1103 5. Tyler, R. *et al.* Vagus Nerve Stimulation Paired with Tones for the Treatment of Tinnitus: A
1104 Prospective Randomized Double-blind Controlled Pilot Study in Humans. *Sci Rep* **7**, 11960
1105 (2017).
1106 6. Dawson, J. *et al.* Vagus nerve stimulation paired with rehabilitation for upper limb motor
1107 function after ischaemic stroke (VNS-REHAB): a randomised, blinded, pivotal, device trial.
1108 *The Lancet* **397**, 1545–1553 (2021).
1109 7. Pruitt, D. T. *et al.* Vagus Nerve Stimulation Delivered with Motor Training Enhances
1110 Recovery of Function after Traumatic Brain Injury. *J. Neurotrauma* **33**, 871–879 (2016).
1111 8. Ganzer, P. D. *et al.* Closed-loop neuromodulation restores network connectivity and motor
1112 control after spinal cord injury. *Elife* **7**, (2018).
1113 9. Meyers, E. C. *et al.* Enhancing plasticity in central networks improves motor and sensory
1114 recovery after nerve damage. *Nat Commun* **10**, 5782 (2019).
1115 10. Kimberley, T. J. *et al.* Vagus Nerve Stimulation Paired With Upper Limb Rehabilitation
1116 After Chronic Stroke. *Stroke* **49**, 2789–2792 (2018).
1117 11. Krahl, S. E., Clark, K. B., Smith, D. C. & Browning, R. A. Locus coeruleus lesions suppress
1118 the seizure-attenuating effects of vagus nerve stimulation. *Epilepsia* **39**, 709–714 (1998).

1119 12. Beaumont, E. *et al.* Cervical vagus nerve stimulation augments spontaneous discharge in
1120 second- and higher-order sensory neurons in the rat nucleus of the solitary tract. *Am J*
1121 *Physiol Heart Circ Physiol* **313**, H354–H367 (2017).
1122 13. Hulsey, D. R. *et al.* Parametric characterization of neural activity in the locus coeruleus in
1123 response to vagus nerve stimulation. *Exp. Neurol.* **289**, 21–30 (2017).
1124 14. Collins, L., Boddington, L., Steffan, P. J. & McCormick, D. Vagus nerve stimulation induces
1125 widespread cortical and behavioral activation. *Current Biology* **31**, 2088-2098.e3 (2021).
1126 15. Hulsey, D. R. *et al.* Reorganization of Motor Cortex by Vagus Nerve Stimulation Requires
1127 Cholinergic Innervation. *Brain Stimul* **9**, 174–181 (2016).
1128 16. Hulsey, D. R., Shedd, C. M., Sarker, S. F., Kilgard, M. P. & Hays, S. A. Norepinephrine
1129 and serotonin are required for vagus nerve stimulation directed cortical plasticity. *Exp.*
1130 *Neurol.* **320**, 112975 (2019).
1131 17. Conner, J. M., Kulczycki, M. & Tuszynski, M. H. Unique Contributions of Distinct
1132 Cholinergic Projections to Motor Cortical Plasticity and Learning. *Cereb Cortex* **20**, 2739–
1133 2748 (2010).
1134 18. Hangya, B., Ranade, S. P., Lorenc, M. & Kepecs, A. Central Cholinergic Neurons Are
1135 Rapidly Recruited by Reinforcement Feedback. *Cell* **162**, 1155–1168 (2015).
1136 19. Zhang, K., Chen, C. D. & Monosov, I. E. Novelty, salience, and surprise-timing are
1137 signaled by neurons in the basal forebrain. *Curr Biol* **29**, 134-142.e3 (2019).
1138 20. Chase, M. H., Sterman, M. B. & Clemente, C. D. Cortical and subcortical patterns of
1139 response to afferent vagal stimulation. *Exp. Neurol.* **16**, 36–49 (1966).
1140 21. Fraschini, M. *et al.* VNS induced desynchronization in gamma bands correlates with
1141 positive clinical outcome in temporal lobe pharmacoresistant epilepsy. *Neurosci. Lett.* **536**,
1142 14–18 (2013).
1143 22. Usami, K. *et al.* Modulation of cortical synchrony by vagus nerve stimulation in adult rats.
1144 *Conf Proc IEEE Eng Med Biol Soc* **2013**, 5348–5351 (2013).

1145 23. Engineer, N. D. *et al.* Reversing pathological neural activity using targeted plasticity.
1146 *Nature* **470**, 101–104 (2011).
1147 24. Porter, B. A. *et al.* Repeatedly pairing vagus nerve stimulation with a movement
1148 reorganizes primary motor cortex. *Cereb. Cortex* **22**, 2365–2374 (2012).
1149 25. Mughrabi, I. T. *et al.* Development and characterization of a chronic implant mouse model
1150 for vagus nerve stimulation. *eLife* **10**, e61270 (2021).
1151 26. Feldman, D. E. The spike timing dependence of plasticity. *Neuron* **75**, 556–571 (2012).
1152 27. Dayan, P. & Balleine, B. W. Reward, Motivation, and Reinforcement Learning. *Neuron* **36**,
1153 285–298 (2002).
1154 28. Leong, Y. C., Radulescu, A., Daniel, R., DeWoskin, V. & Niv, Y. Dynamic Interaction
1155 between Reinforcement Learning and Attention in Multidimensional Environments. *Neuron*
1156 **93**, 451–463 (2017).
1157 29. Peters, A. J., Lee, J., Hedrick, N. G., O'Neil, K. & Komiyama, T. Reorganization of
1158 corticospinal output during motor learning. *Nat. Neurosci.* **20**, 1133–1141 (2017).
1159 30. Padmashri, R. & Dunaevsky, A. Modulation of excitatory but not inhibitory synaptic inputs
1160 in the mouse primary motor cortex in the late phase of motor learning. *Neurosci Lett* **709**,
1161 134371 (2019).
1162 31. Censor, N., Sagi, D. & Cohen, L. G. Common mechanisms of human perceptual and motor
1163 learning. *Nat Rev Neurosci* **13**, 658–664 (2012).
1164 32. Wickens, J. R., Reynolds, J. N. & Hyland, B. I. Neural mechanisms of reward-related motor
1165 learning. *Current Opinion in Neurobiology* **13**, 685–690 (2003).
1166 33. Guo, W., Robert, B. & Polley, D. B. The Cholinergic Basal Forebrain Links Auditory Stimuli
1167 with Delayed Reinforcement to Support Learning. *Neuron* **103**, 1164-1177.e6 (2019).
1168 34. Ramanathan, D., Tuszynski, M. H. & Conner, J. M. The Basal Forebrain Cholinergic
1169 System Is Required Specifically for Behaviorally Mediated Cortical Map Plasticity. *J.*
1170 *Neurosci.* **29**, 5992–6000 (2009).

1171 35. Ramanathan, D. S., Conner, J. M., Anilkumar, A. A. & Tuszynski, M. H. Cholinergic
1172 systems are essential for late-stage maturation and refinement of motor cortical circuits. *J*
1173 *Neurophysiol* **113**, 1585–1597 (2015).
1174 36. Kucinski, A., Kim, Y. & Sarter, M. Basal forebrain chemogenetic inhibition disrupts the
1175 superior complex movement control of goal-tracking rats. *Behav. Neurosci.* **133**, 121–134
1176 (2019).
1177 37. Gielow, M. R. & Zaborszky, L. The Input-Output Relationship of the Cholinergic Basal
1178 Forebrain. *Cell Reports* **18**, 1817–1830 (2017).
1179 38. Do, J. P. *et al.* Cell type-specific long-range connections of basal forebrain circuit. *eLife* **5**,
1180 e13214 (2016).
1181 39. Lima, S. Q., Hromádka, T., Znamenskiy, P. & Zador, A. M. PINP: A New Method of
1182 Tagging Neuronal Populations for Identification during In Vivo Electrophysiological
1183 Recording. *PLoS One* **4**, e6099 (2009).
1184 40. Bowles, S., Williamson, W. R., Nettles, D., Hickman, J. & Welle, C. G. Closed-loop
1185 automated reaching apparatus (CLARA) for interrogating complex motor behaviors. *J.*
1186 *Neural Eng.* (2021) doi:10.1088/1741-2552/ac1ed1.
1187 41. Shmuelof, L., Krakauer, J. W. & Mazzoni, P. How is a motor skill learned? Change and
1188 invariance at the levels of task success and trajectory control. *Journal of Neurophysiology*
1189 **108**, 578–594 (2012).
1190 42. Kawai, R. *et al.* Motor cortex is required for learning but not executing a motor skill. *Neuron*
1191 **86**, 800–812 (2015).
1192 43. Guo, J.-Z. *et al.* Cortex commands the performance of skilled movement. *eLife* **4**, e10774
1193 (2015).
1194 44. Donoghue, J. P. & Sanes, J. N. Motor areas of the cerebral cortex. *J Clin Neurophysiol* **11**,
1195 382–396 (1994).

45. Sanes, J. N. & Donoghue, J. P. Plasticity and primary motor cortex. *Annu Rev Neurosci* **23**, 393–415 (2000).

46. Peters, A. J., Chen, S. X. & Komiyama, T. Emergence of reproducible spatiotemporal activity during motor learning. *Nature* **510**, 263–267 (2014).

47. Levy, S. *et al.* Cell-Type-Specific Outcome Representation in the Primary Motor Cortex. *Neuron* **107**, 954-971.e9 (2020).

48. Borland, M. S. *et al.* Cortical Map Plasticity as a Function of Vagus Nerve Stimulation Intensity. *Brain Stimulation* **9**, 117–123 (2016).

49. Reed, A. *et al.* Cortical map plasticity improves learning but is not necessary for improved performance. *Neuron* **70**, 121–131 (2011).

50. Han, W. *et al.* A Neural Circuit for Gut-Induced Reward. *Cell* **175**, 887–888 (2018).

51. Neuser, M. P. *et al.* Vagus nerve stimulation boosts the drive to work for rewards. *Nat Commun* **11**, 3555 (2020).

52. Weber, I. *et al.* Trust your gut: vagal nerve stimulation in humans improves reinforcement learning. *Brain Communications* **3**, (2021).

53. Pekny, S. E., Izawa, J. & Shadmehr, R. Reward-Dependent Modulation of Movement Variability. *J. Neurosci.* **35**, 4015–4024 (2015).

54. Uehara, S., Mawase, F., Therrien, A. S., Cherry-Allen, K. M. & Celnik, P. Interactions between motor exploration and reinforcement learning. *Journal of Neurophysiology* **122**, 797–808 (2019).

55. Wolpert, D. M., Diedrichsen, J. & Flanagan, J. R. Principles of sensorimotor learning. *Nat Rev Neurosci* **12**, 739–751 (2011).

56. Athalye, V. R., Santos, F. J., Carmena, J. M. & Costa, R. M. Evidence for a neural law of effect. *Science* **359**, 1024–1029 (2018).

57. Oby, E. R. *et al.* New neural activity patterns emerge with long-term learning. *Proc Natl Acad Sci U S A* **116**, 15210–15215 (2019).

1222 58. Aronov, D., Andalman, A. S. & Fee, M. S. A Specialized Forebrain Circuit for Vocal
1223 Babbling in the Juvenile Songbird. *Science* **320**, 630–634 (2008).
1224 59. Garst-Orozco, J., Babadi, B. & Ölveczky, B. P. A neural circuit mechanism for regulating
1225 vocal variability during song learning in zebra finches. *eLife* **3**, e03697 (2014).
1226 60. Dhawale, A. K., Smith, M. A. & Ölveczky, B. P. The Role of Variability in Motor Learning.
1227 *Annu Rev Neurosci* **40**, 479–498 (2017).
1228 61. Wu, H. G., Miyamoto, Y. R., Castro, L. N. G., Ölveczky, B. P. & Smith, M. A. Temporal
1229 structure of motor variability is dynamically regulated and predicts motor learning ability.
1230 *Nat Neurosci* **17**, 312–321 (2014).
1231 62. Athalye, V. R., Ganguly, K., Costa, R. M. & Carmena, J. M. Emergence of Coordinated
1232 Neural Dynamics Underlies Neuroprosthetic Learning and Skillful Control. *Neuron* **93**, 955-
1233 970.e5 (2017).
1234 63. Dhawale, A. K., Miyamoto, Y. R., Smith, M. A. & Ölveczky, B. P. Adaptive Regulation of
1235 Motor Variability. *Current Biology* **29**, 3551-3562.e7 (2019).
1236 64. Perez, S. M., Carreno, F. R., Frazer, A. & Lodge, D. J. Vagal Nerve Stimulation Reverses
1237 Aberrant Dopamine System Function in the Methylazoxymethanol Acetate Rodent Model
1238 of Schizophrenia. *J Neurosci* **34**, 9261–9267 (2014).
1239 65. Farrand, A. Q. *et al.* Vagus nerve stimulation improves locomotion and neuronal
1240 populations in a model of Parkinson's disease. *Brain Stimul* **10**, 1045–1054 (2017).
1241 66. Sawaki, L. *et al.* Cholinergic Influences on Use-Dependent Plasticity. *Journal of*
1242 *Neurophysiology* **87**, 166–171 (2002).
1243 67. Shinoe, T., Matsui, M., Taketo, M. M. & Manabe, T. Modulation of Synaptic Plasticity by
1244 Physiological Activation of M1 Muscarinic Acetylcholine Receptors in the Mouse
1245 Hippocampus. *J Neurosci* **25**, 11194–11200 (2005).
1246 68. Kang, J. I., Huppé-Gourgues, F. & Vaucher, E. Boosting visual cortex function and
1247 plasticity with acetylcholine to enhance visual perception. *Front. Syst. Neurosci.* **8**, (2014).

1248 69. Jiang, L. *et al.* Cholinergic signaling controls conditioned-fear behaviors and enhances
1249 plasticity of cortical-amygdala circuits. *Neuron* **90**, 1057–1070 (2016).
1250 70. Lin, S.-C. & Nicolelis, M. A. L. Neuronal ensemble bursting in the basal forebrain encodes
1251 salience irrespective of valence. *Neuron* **59**, 138–149 (2008).
1252 71. Conner, J. M., Culberson, A., Packowski, C., Chiba, A. A. & Tuszynski, M. H. Lesions of
1253 the Basal Forebrain Cholinergic System Impair Task Acquisition and Abolish Cortical
1254 Plasticity Associated with Motor Skill Learning. *Neuron* **38**, 819–829 (2003).
1255 72. Puzerey, P. A., Maher, K., Prasad, N. & Goldberg, J. H. Vocal learning in songbirds
1256 requires cholinergic signaling in a motor cortex-like nucleus. *Journal of Neurophysiology*
1257 **120**, 1796–1806 (2018).
1258 73. Détári, L., Juhász, G. & Kukorelli, T. Effect of stimulation of vagal and radial nerves on
1259 neuronal activity in the basal forebrain area of anaesthetized cats. *Acta Physiol Hung* **61**,
1260 147–154 (1983).
1261 74. Smiley, J. F., Subramanian, M. & Mesulam, M.-M. Monoaminergic–cholinergic interactions
1262 in the primate basal forebrain. *Neuroscience* **93**, 817–829 (1999).
1263 75. Zaborszky, L., Rosin, D. L. & Kiss, J. Alpha-adrenergic receptor (alpha(2 A)) is colocalized
1264 in basal forebrain cholinergic neurons: a light and electron microscopic double
1265 immunolabeling study. *J Neurocytol* **33**, 265–276 (2004).
1266 76. Schwarz, L. A. & Luo, L. Organization of the Locus Coeruleus-Norepinephrine System.
1267 *Current Biology* **25**, R1051–R1056 (2015).
1268 77. Groves, D. A., Bowman, E. M. & Brown, V. J. Recordings from the rat locus coeruleus
1269 during acute vagal nerve stimulation in the anaesthetised rat. *Neuroscience Letters* **379**,
1270 174–179 (2005).
1271 78. Whishaw, I. Q., O'Connor, W. T. & Dunnett, S. B. THE CONTRIBUTIONS OF MOTOR
1272 CORTEX, NIGROSTRIATAL DOPAMINE AND CAUDATE-PUTAMEN TO SKILLED
1273 FORELIMB USE IN THE RAT. *Brain* **109**, 805–843 (1986).

1274 79. Lemon, R. N. Descending Pathways in Motor Control. *Annual Review of Neuroscience* **31**,
1275 195–218 (2008).
1276 80. Adler, A., Zhao, R., Shin, M. E., Yasuda, R. & Gan, W.-B. Somatostatin-Expressing
1277 Interneurons Enable and Maintain Learning-Dependent Sequential Activation of Pyramidal
1278 Neurons. *Neuron* **102**, 202-216.e7 (2019).
1279 81. Biane, J. S., Takashima, Y., Scanziani, M., Conner, J. M. & Tuszynski, M. H.
1280 Reorganization of Recurrent Layer 5 Corticospinal Networks Following Adult Motor
1281 Training. *J Neurosci* **39**, 4684–4693 (2019).
1282 82. Luft, A. R. & Schwarz, S. Dopaminergic signals in primary motor cortex. *International*
1283 *Journal of Developmental Neuroscience* **27**, 415–421 (2009).
1284 83. Hosp, J. A., Pekanovic, A., Rioult-Pedotti, M. S. & Luft, A. R. Dopaminergic Projections
1285 from Midbrain to Primary Motor Cortex Mediate Motor Skill Learning. *J. Neurosci.* **31**,
1286 2481–2487 (2011).
1287 84. Heffley, W. *et al.* Coordinated cerebellar climbing fiber activity signals learned
1288 sensorimotor predictions. *Nat Neurosci* **21**, 1431–1441 (2018).
1289 85. Eggermann, E., Kremer, Y., Crochet, S. & Petersen, C. C. H. Cholinergic signals in mouse
1290 barrel cortex during active whisker sensing. *Cell Rep* **9**, 1654–1660 (2014).
1291 86. Reimer, J. *et al.* Pupil fluctuations track rapid changes in adrenergic and cholinergic activity
1292 in cortex. *Nat Commun* **7**, 13289 (2016).
1293 87. Musall, S., Urai, A. E., Sussillo, D. & Churchland, A. K. Harnessing behavioral diversity to
1294 understand neural computations for cognition. *Current Opinion in Neurobiology* **58**, 229–
1295 238 (2019).
1296 88. Lai, J. & David, S. V. Short-Term Effects of Vagus Nerve Stimulation on Learning and
1297 Evoked Activity in Auditory Cortex. *eNeuro* **8**, (2021).

89. Nitsche, M. A. *et al.* Facilitation of implicit motor learning by weak transcranial direct current stimulation of the primary motor cortex in the human. *J Cogn Neurosci* **15**, 619–626 (2003).

90. Khanna, P. *et al.* Low-frequency stimulation enhances ensemble co-firing and dexterity after stroke. *Cell* **184**, 912-930.e20 (2021).

91. Potok, W., Bächinger, M., Groen, O. van der, Cretu, A. L. & Wenderoth, N. Transcranial Random Noise Stimulation Acutely Lowers the Response Threshold of Human Motor Circuits. *J. Neurosci.* **41**, 3842–3853 (2021).

92. Fritsch, B. *et al.* Direct current stimulation promotes BDNF-dependent synaptic plasticity: Potential implications for motor learning. *Neuron* **66**, 198–204 (2010).

93. Ammann, C., Spampinato, D. & Márquez-Ruiz, J. Modulating Motor Learning through Transcranial Direct-Current Stimulation: An Integrative View. *Front Psychol* **7**, 1981 (2016).

94. Kang, E. K., Kim, Y. K., Sohn, H. M., Cohen, L. G. & Paik, N.-J. Improved picture naming in aphasia patients treated with cathodal tDCS to inhibit the right Broca's homologue area. *Restor Neurol Neurosci* **29**, 141–152 (2011).

95. Stagg, C. J. *et al.* Polarity and timing-dependent effects of transcranial direct current stimulation in explicit motor learning. *Neuropsychologia* **49**, 800–804 (2011).

96. Albuquerque, L. L. de *et al.* An acute application of transcranial random noise stimulation does not enhance motor skill acquisition or retention in a golf putting task. *Human Movement Science* **66**, 241–248 (2019).

97. Rossi, J. *et al.* Melanocortin-4-receptors Expressed by Cholinergic Neurons Regulate Energy Balance and Glucose Homeostasis. *Cell Metab* **13**, 195–204 (2011).

98. Zhao, S. *et al.* Cell-type Specific Optogenetic Mice for Dissecting Neural Circuitry Function. *Nat Methods* **8**, 745–752 (2011).

99. Whishaw, I. Q., Whishaw, P. & Gorny, B. The Structure of Skilled Forelimb Reaching in the Rat: A Movement Rating Scale. *J Vis Exp* 816 (2008) doi:10.3791/816.

100. Riekkinen, P., Sirviö, J., Aaltonen, M. & Riekkinen, P. Effects of concurrent manipulations of nicotinic and muscarinic receptors on spatial and passive avoidance learning. *Pharmacol Biochem Behav* **37**, 405–410 (1990).

101. Riekkinen, P., Riekkinen, M. & Sirviö, J. Cholinergic drugs regulate passive avoidance performance via the amygdala. *J Pharmacol Exp Ther* **267**, 1484–1492 (1993).

102. Prus, A. J., James, J. R. & Rosecrans, J. A. Conditioned Place Preference. in *Methods of Behavior Analysis in Neuroscience* (ed. Buccafusco, J. J.) (CRC Press/Taylor & Francis, 2009).

103. Li, Q. *et al.* Refinement of learned skilled movement representation in motor cortex deep output layer. *Nature Communications* **8**, 15834 (2017).

104. Schmitzer-Torbert, N., Jackson, J., Henze, D., Harris, K. & Redish, A. D. Quantitative measures of cluster quality for use in extracellular recordings. *Neuroscience* **131**, 1–11 (2005).

105. Pnevmatikakis, E. A. & Giovannucci, A. NoRMCorre: An online algorithm for piecewise rigid motion correction of calcium imaging data. *J Neurosci Methods* **291**, 83–94 (2017).

106. Zhou, P. *et al.* Efficient and accurate extraction of in vivo calcium signals from microendoscopic video data. *eLife* **7**, e28728 (2018).

107. Jimenez, J. C. *et al.* Anxiety Cells in a Hippocampal-Hypothalamic Circuit. *Neuron* **97**, 670-683.e6 (2018).

108. Sheintuch, L. *et al.* Tracking the Same Neurons across Multiple Days in Ca2+ Imaging Data. *Cell Rep* **21**, 1102–1115 (2017).